

Faster MCMC for Gaussian Latent Position Network Models

Neil A. Spencer*, Brian Junker

Department of Statistics and Data Science, Carnegie Mellon University,
and

Tracy M. Sweet

Department of Human Development and Quantitative Methodology
University of Maryland

June 16, 2020

Abstract

Latent position network models are a versatile tool in network science; applications include clustering entities, controlling for causal confounders, and defining priors over unobserved graphs. Estimating each node's latent position is typically framed as a Bayesian inference problem, with Metropolis within Gibbs being the most popular tool for approximating the posterior distribution. However, it is well-known that Metropolis within Gibbs is inefficient for large networks; the acceptance ratios are expensive to compute, and the resultant posterior draws are highly correlated. In this article, we propose an alternative Markov chain Monte Carlo strategy—defined using a combination of split Hamiltonian Monte Carlo and Firefly Monte Carlo—that leverages the posterior distribution's functional form for more efficient posterior computation. We demonstrate that these strategies outperform Metropolis within Gibbs and other algorithms on synthetic networks, as well as on real information-sharing networks of teachers and staff in a school district.

Keywords: Hamiltonian Monte Carlo, Network Data, Firefly Monte Carlo, Latent Space Model, Longitudinal Network Data, Bayesian Computation

*All three authors gratefully acknowledge funding from IES (US Dept of ED) Award 305D150045, NAS gratefully acknowledges an NSERC Postgraduate Scholarship, and funding from National Institute of Mental Health grant R01MH064537

1 Introduction

Network data—measurements of relationships across sets of entities—are becoming increasingly common across science and industry, largely due to technological advances in data collection and storage. Common sources of network data include social networks [Carrington et al., 2005], citation networks [Ji and Jin, 2016], gene regulatory networks [Hecker et al., 2009], disease transmission networks [Newman, 2002], neural connectomes [Chen et al., 2016], transportation networks [Xie and Levinson, 2009], and food webs [Chiu and Westveld, 2011]. A broad range of statistical tools based on stochastic graphs [Goldenberg et al., 2010, Crane, 2018] are available for probabilistically modeling networks, ranging from the simple Erdős-Renyi model [Erdős and Rényi, 1960] to sophisticated latent variable models (e.g. Airoldi et al. [2008], Clauset et al. [2008], Fosdick et al. [2018], Dabbs et al. [2020]). Latent variable models can be defined to capture common network properties such as community structure, hierarchical structure, and degree heterogeneity.

In latent variable models—like most network models that model edges as random variables—the computational complexity of evaluating the likelihood is quadratic in the number of nodes. These models are thus computationally costly to fit to large networks, especially if one wishes to quantify uncertainty in a Bayesian modeling and inference framework [Gelman et al., 2013]. For instance, traditional Markov chain Monte Carlo algorithms [Gamerman and Lopes, 2006] (e.g. Gibbs sampling, random walk Metropolis, or Metropolis within Gibbs) can require tens of thousands of likelihood evaluations to accurately quantify expectations and uncertainties. This computational burden is even larger when the chains are slow-mixing, which is often the case for Bayesian hierarchical models.

In this work, we develop a faster Markov chain Monte Carlo algorithm for a class of latent variable network models called the latent position network model (LPM). LPMs—originally proposed by Hoff et al. [2002]—have been applied to a variety of statistical problems, including modeling network interventions [Sweet et al., 2013], clustering entities [Handcock et al., 2007], modeling social influence [Sweet and Adhikari, 2020], controlling for causal confounders [Shalizi and McFowland III, 2016], and defining priors on unobserved graphs [Linderman et al., 2016]. Each node in a LPM possesses a real-valued latent variable

(its *position*), with each edge treated as an independent Bernoulli random draw depending on the participating nodes' latent positions. These probabilities are modeled as a decreasing function of the nodes' latent distance, thus promoting homophily and triadic closure (e.g. a friend of a friend is more likely to be a friend) across the network. Edge probabilities may also depend on covariates, such as whether the entities share a common observed trait.

The principal task in fitting a LPM is to infer the latent positions (and thus the latent distances between pairs of nodes), as well as the parameters of the link function (e.g. the effect of any covariates). In a Bayesian modeling and inference framework, the posterior distribution of these parameters quantifies uncertainty in the corresponding estimates. Evaluating and summarizing the posterior distribution requires intensive computation—its normalization constant is defined by an integral that lacks closed form and is thus intractable to evaluate exactly.

The standard tool for computing posterior summaries has been Markov chain Monte Carlo (MCMC) via Metropolis within Gibbs [Handcock et al., 2007, Raftery et al., 2012]. This technique avoids the need to calculate the normalization constant of the posterior, and can approximate posterior expectations arbitrarily well if the chain is long enough. However, accurate inference via Metropolis within Gibbs can be computationally infeasible for large networks. This infeasibility is largely due to two phenomena: (1) The random walk step size required to obtain high acceptance rates shrinks as the number of nodes grows, resulting in slowly mixing chains with strong autocorrelation, and (2) the computational complexity of performing a full sweep of position updates is quadratic in the number of nodes, so each iteration for a large network is expensive to compute. We address these challenges in this article through the development of a more efficient MCMC algorithm.

We are not the first to recognize these problems, nor are we the first to propose solutions. In recent years, multiple approaches for approximating the likelihood have been proposed to successfully scale up Bayesian inference of LPMs to large networks. Raftery et al. [2012] proposed a case-control based approach, sub-sampling the non-edge dyads to approximate each acceptance ratio in Metropolis within Gibbs. Rastelli et al. [2018] proposed a discrete-grid approximation of the latent positions, simplifying each likelihood evaluation. Salter-

Townshend and Murphy [2013] proposed the use of variational inference as an alternative to MCMC. Though each of these approaches speeds up posterior inference, the improvements come at the cost of biasing the results with the likelihood approximations. As such, these methods do not have the same asymptotic guarantees as the traditional Metropolis within Gibbs approach. Regardless of how long the chain is run, a bias persists. In this respect, our work differs previous approaches; our faster MCMC algorithm is exact.

The main tool we use to accomplish this task is Hamiltonian Monte Carlo (HMC). HMC [Duane et al., 1987, Neal, 2011, Betancourt, 2017] and its variants [Girolami and Calderhead, 2011, Hoffman and Gelman, 2014, Betancourt, 2016] are a class of MCMC algorithms that leverage Hamiltonian dynamics to construct efficient gradient-informed proposals for differentiable posterior distributions. A properly tuned HMC proposal produces large moves in a chain whilst maintaining high Metropolis-Hastings acceptance rates. As such, HMC is often much more efficient than traditional random walk-based methods, especially for high-dimensional distributions with strong correlations amongst the variables.

Over the past few years, the use of HMC algorithms for Bayesian inference has been democratized in the open source software Stan [Carpenter et al., 2017]. Stan implements a specialized tuning and sampling strategy for HMC that is robust across a broad class of Bayesian models. Built-in diagnostic tools make it easy to identify and address mixing problems within the Markov chain. Nevertheless, Stan’s robustness depends on making some sacrifices (e.g. all variables must be updated simultaneously, and discrete latent variables must be marginalized). Usually, this rigidity is worthwhile; the limited scope of Stan’s algorithm still covers a wide range of models, and can be a relatively small price to pay for the ease of implementation and built-in mixing diagnostics. However, this is not the case for large LPMs; MCMC for large LPMs often stretches one’s computational resources to their limit. We thus need all tools at our disposal (including sampling discrete random variables and block updates of variables) to optimize our inference strategy.

The specialized HMC-based sampling strategy we present in this article is specifically intended for Gaussian LPMs [Rastelli et al., 2016], a class of LPMs for which the link probability function decays like a half-Gaussian probability density function. This class of

LPMs was originally studied because they are easy to work with analytically. We show here that the Gaussian-inspired link function also provides computational advantages—the log posterior can be split into Gaussian and non-Gaussian components, thus facilitating efficient integration of HMC via split HMC [Shahbaba et al., 2014]. Moreover, we further increase the efficiency for sparse networks by developing an exact dyad subsampling scheme based on Firefly Monte Carlo (FlyMC [Maclaurin and Adams, 2015]). This scheme allows us to subsample that non-edge dyads, decreasing the complexity of the non-Gaussian component of the posterior while maintaining an exact MCMC strategy. To ensure a complete LPM fitting algorithm, we also including Markov chain updates for the parameters of the link function, and show that the FlyMC approach can simplify inferring the sparsity parameters. Our approach is compatible with inferring the effect of categorical covariates on the link, as well as incorporating prior dependence between latent positions in the network (e.g. as in longitudinal latent position models [Kim et al., 2018]).

The remainder of the article is organized as follows. Section 2 establishes notation and provides the necessary background information pertaining to LPMs, Gaussian LPMs and Hamiltonian Monte Carlo. Section 3 outlines the ingredients of our new computation methodology for Gaussian LPMs: split Hamiltonian Monte Carlo and firefly Monte Carlo, then combines them with updates to the link function parameters to define a new Markov chain Monte Carlo strategy. Section 4 describes a metric for assessing the efficiency Monte Carlo algorithms for LPMs, then presents two empirical studies to demonstrate the superiority of our algorithm. Study 1 uses synthetically-generated examples to demonstrate the superior performance of our method compared to a variety of existing approaches in the literature such as Metropolis within Gibbs, elliptical slice sampling, Stan, and the No-U-turn sampler. Study 2 demonstrates the extent to which our algorithms outperform Metropolis within Gibbs for fitting information-sharing models amongst teachers and staff in a school district. Section 5 contains some concluding remarks.

2 Preliminaries

The following notation will be used throughout the paper. We use \mathbb{R} to denote the set of real numbers, \mathbb{R}_+ to denote the set of non-negative real numbers, \mathbb{N} to denote the set of natural numbers, and $[n]$ to denote the set $\{1, \dots, n\}$ of natural numbers less than or equal to n . For a set S , we use S^d to denote the collection of all d -length vectors with entries from S and $S^{n \times d}$ to denote collection of possible $n \times d$ matrices with entries from S . For two sets S_1, S_2 , $S_1 \times S_2$ denotes their Cartesian product.

For a vector $z \in \mathbb{R}^d$, z_i denotes its i th entry and $\|z\|$ denote its Euclidean norm. For a matrix $B \in \mathbb{R}^{n \times d}$, $B_{i \cdot}$ denotes its i th row, $B_{\cdot i}$ denotes its i th column, B_{ij} denote its (i, j) th entry, $B^T \in \mathbb{R}^{d \times n}$ denotes its transpose, $\|B\|$ denotes its Frobenius norm, and B^{-1} denotes its inverse. We use I_n to denote the $n \times n$ identity matrix.

We represent networks among n entities as undirected binary graphs on n nodes. We use $A \in \{0, 1\}^{n \times n}$ to denote the adjacency matrix of the graph, with $A_{ij} = 1$ indicating the presence of an edge between nodes i and j , and $A_{ij} = 0$ indicating its absence. Our focus is on undirected graphs, so $A_{ij} = A_{ji}$ for all dyads $(i, j) \in [n]^2$. For simplicity, we use A to refer to both a graph and its adjacency matrix interchangeably, using $[n]$ index the nodes according to the order of their rows in the adjacency matrix. We use the shorthand $E_A \subseteq [n]^2$ to denote the set of edges associated with A , and $\{(i, j) \notin E_A\}$ to denote the set of possible edges absent from E_A . The combinatorial Laplacian of A is denoted as $L^A \in \mathbb{R}^{n \times n}$. Specifically, $L^A = D^A - A$ where D^A is a diagonal matrix of the node degrees $D_{ii}^A = \sum_{j=1}^n A_{ij}$.

2.1 Latent Position Network Models

In a distance-based latent position network model (LPM) of [Hoff et al., 2002], each node $i \in [n]$ is modeled as having a d -dimensional latent position $z_i \in \mathbb{R}^d$ for some positive integer d (typically chosen to be 2 or 3 in practice to facilitate visualization). It is convenient (for notation and computation) to arrange these latent positions in a matrix $Z \in \mathbb{R}^{n \times d}$, where

$Z_{i\cdot} = z_i$. The edges A_{ij} are modeled as being generated according to

$$\mathbb{P}(A_{ij} = 1|Z) = K(\|z_i - z_j\|, x_{ij}) \quad (1)$$

where $\|z_i - z_j\|$ denotes the distance between nodes i and j , x_{ij} represents any relevant edge-specific covariates for nodes i and j , and K is the *link function*—a non-increasing function from the product of $\mathbb{R}_+ \times \mathcal{X}$ to $[0, 1]$. Here, \mathcal{X} denotes the range of possible values of the covariate x_{ij} for each dyad $(i, j) \in [n]^2$.

In this article, we focus on the case where each covariate x_{ij} is categorical, taking on of $C \in \mathbb{N}$ distinct values (without loss of generality, we use $\mathcal{X} = [C]$ to encode the categories of such variables). Categorical covariates are common in applied problems. For example, the school district information-sharing network [Spillane et al., 2018, Sweet and Adhikari, 2020] considered in Section 4.3 involves a binary covariate ($C = 2$) indicating whether or not each pair of individuals work in the same school ($x_{ij} = 1$ if individuals i and j work at the same school, and $x_{ij} = 2$ otherwise). Similarly, the classroom example of Hoff et al. [2002] involves a covariate indicating whether or not pupils are of the same sex. We use $x \in [C]^{n \times n}$ to refer to the collection of all $(x_{ij})_{i \in [n], j \in [n]}$. If no covariates are present for a model, then x simply collapses to a $n \times n$ matrix of ones. Extending the techniques we describe here to accommodate real-valued covariates is a potential avenue for future work.

In their original version of the LPM, Hoff et al. [2002] proposed modeling K as a logistic function of the latent distance and the covariate according to

$$K(\|z_i - z_j\|, x_{ij}) = (1 + \exp(\alpha + \beta_{x_{ij}} + \|z_i - z_j\|))^{-1}. \quad (2)$$

Here, the parameters $\alpha \in \mathbb{R}$ and $\beta \in \mathbb{R}^C$ control the total number of edges and the effect of the covariates, respectively. Recently, Rastelli et al. [2016] proposed an alternative form for K inspired by the functional form of the Gaussian probability density function—aptly named the Gaussian Latent Position Model (GLPM). Their original exposition did not consider covariates, taking the form

$$K(\|z_i - z_j\|) = \tau \exp\left(-\frac{1}{2\gamma^2} \|z_i - z_j\|^2\right). \quad (3)$$

Here, the parameter $\tau \in [0, 1]$ controls the number of edges (i.e. sparsity level) in the network and $\gamma^2 > 0$ controls the decay of the link probabilities. Thus far, two advantages

of GLPMs over logistic LPMs have been identified in the literature. The Gaussian-like choice of K yields closed-form expressions for various network statistics of GLPMs (such as the average degree of a node and its neighbors) making them easier to theoretically analyze than logistic LPMs [Rastelli et al., 2016]. Moreover, the lighter tails of the Gaussian link function are conducive to proving consistency of the maximum likelihood estimator of the latent positions [Spencer and Shalizi, 2019].

In this paper, we identify and explore yet another advantage of GLPMs—the Gaussian shape of K facilitates faster posterior inference techniques. Our work considers an extension of the GLPM to accommodate categorical covariates. Specifically, we consider

$$K(\|z_i - z_j\|, x_{ij}) = \tau_{x_{ij}} \exp\left(-\frac{1}{2\gamma^2}\|z_i - z_j\|^2\right), \quad (4)$$

with parameters $\tau \in [0, 1]^C$ and $\gamma^2 > 0$. Here, the effect of the covariate is encoded in the vector τ , allowing for subnetworks corresponding to some levels of the covariate categories to be far sparser than others. This single covariate formulation can be extended without loss of generality to multiple discrete covariates, with or without interactions, by a suitable mapping of the joint range space of covariates into $[C]$. For notational conciseness, we occasionally omit the dependence of K on x_{ij} in this article. Together, the Gaussian shape and factorizability of K can be exploited to speed up Bayesian inference.

2.2 Bayesian Inference for LPMs

Fitting a LPM to a graph A can be separated into two interdependent tasks: (1) inferring the latent positions $Z \in \mathbb{R}^{n \times d}$ of the nodes, and (2) inferring the parameters of the link function K (e.g. τ , γ^2 for the Gaussian link). Depending on the modeling objective of the problem at hand, either (1) or (2) could be the primary inferential target. For instance, Z is primary inferential target when controlling for causal confounders [Shalizi and McFowland III, 2016], but τ is the primary target when estimating the effect of a covariate on edge probabilities. Regardless, both inference tasks are typically carried out simultaneously in a Monte Carlo single algorithm; independent priors are placed on both the parameters and the latent positions, and their posterior distribution is approximated with samples drawn according to Markov chain Monte Carlo.

To simplify exposition, we will present our strategies for the two inference tasks (inferring Z and inferring K) separately in Sections 3.1 and 3.3. Here, we review existing computational strategies from the literature for inferring the latent positions Z conditional on K . All discussion of inference of the parameters of K for the GLPM is deferred until Section 3.3.

Given the full functional form of the link function K (as well as any covariates x it depends on), Bayesian inference of the latent positions Z depends on two additional inputs: an observed network (encoded by an adjacency matrix $A \in \{0, 1\}^{n \times n}$), and a prior on $Z \in \mathbb{R}^{n \times d}$. The standard prior choice for Z in the literature has been an independent isotropic d -dimensional Gaussian on each row (i.e. latent position) of Z (usually $d = 2$ is used for visualization purposes). Here, we generalize this prior to $Z_{\cdot k} \sim N(0, \Omega^{-1})$ —defined independently for each $k \in [d]$. That is, the nodes’ positions are independent across dimensions, but can be dependent within a dimension. Without loss of generality, any Gaussian prior exhibiting dependence of a nodes’ position across dimensions can be transformed into an equivalent prior with independence across dimensions via a rotation¹.

This more general set-up for the prior allows for known structural information—such as feature-informed node clustering or temporal dependence—to be included as non-zero entries in the precision matrix $\Omega \in \mathbb{R}^{n \times n}$. Other priors, such as a mixture of Multivariate Gaussians [Handcock et al., 2007, Krivitsky et al., 2009], are beyond the scope of this paper, but would involve a straightforward extension of the methods presented here.

Given the prior $Z_{\cdot k} \sim N(0, \Omega^{-1})$ for $k \in [d]$, the posterior distribution on Z is given by

$$\mathbb{P}(Z|A) \propto \prod_{(i,j) \in E_A} K(\|z_i - z_j\|) \prod_{(i,j) \notin E_A} (1 - K(\|z_i - z_j\|)) \exp\left(-\frac{1}{2} \sum_{k=1}^d Z_{\cdot k}^T \Omega Z_{\cdot k}\right). \quad (5)$$

The normalization constant for this density is a $(n \times d)$ -dimensional integral that cannot be computed analytically. Instead, we must rely on approximate methods for calculating expectations with respect to the posterior. Here, we discuss two related Monte Carlo strategies already proposed in the LPM literature, and use their short-comings to motivate our new Hamiltonian Monte Carlo strategy.

¹In this sense, the dimensions of Z behave like principal components in principal component analysis

In their seminal LPM paper, Hoff et al. [2002] proposed for the posterior computation of $\mathbb{P}(Z|A)$ to be carried out via Markov chain Monte Carlo (MCMC). They obtained a Markov Chain Z^1, Z^2, \dots, Z^T with stationary distribution $\mathbb{P}(Z|A)$ by repeatedly applying a random walk Metropolis update to all latent positions Z simultaneously. As is the case for most MCMC algorithms, ensuring an adequate Metropolis-Hastings acceptance rate requires that the standard deviations of these random walk updates be appropriately tuned using a series of short pilot runs. However, these joint random walk proposals are known to be inefficient when the posterior is high-dimensional (e.g. for networks with many nodes) because the random walk standard deviation required to obtain reasonable acceptance rates is simply too small to explore the space efficiently. For example, when fitting GLPMs to synthetically generated 500 node networks ($C = 1$, $\tau = 0.5$, $\gamma^2 = 0.5$), we found that random walk standard deviations below 0.01 are typically required to obtain reasonable acceptance rates.

In an effort to alleviate this slow mixing, the subsequent LPM literature (e.g. [Handcock et al., 2007, Raftery et al., 2012]) use a Metropolis within Gibbs strategy for updating the latent positions instead. In *Metropolis within Gibbs*, the latent positions $(z_i)_{i \in [n]}$ are updated one at a time in sequence according to a random walk via a symmetric kernel q centered at its current position (e.g. a scaled isotropic Gaussian or multivariate uniform). This approach is still widely-used today (e.g. Fosdick et al. [2018], Aliverti and Durante [2019], Sweet and Adhikari [2020]); it is also implemented in the popular R package `latentnet` [Krivitsky and Handcock, 2008].

A sweep of the Metropolis within Gibbs algorithm can be summarized as follows. For each $i \in [n]$,

1. Propose $z'_i \sim q_\delta(z_i, z'_i)$.
2. Accept this proposal with probability equal to

$$\frac{\mathbb{P}(Z'|A)}{\mathbb{P}(Z|A)} = \frac{\exp\left(\sum_{k=1}^d Z_{\cdot k}^T \Omega Z_{\cdot k}\right)}{\exp\left(\sum_{k=1}^d (Z'_{\cdot k})^T \Omega Z'_{\cdot k}\right)} \prod_{j:(i,j) \in E_A} \frac{K(\|z'_i - z_j\|)}{K(\|z_i - z_j\|)} \prod_{j:(i,j) \notin E_A} \frac{1 - K(\|z'_i - z_j\|)}{1 - K(\|z_i - z_j\|)} \quad (6)$$

Otherwise reject and keep z_i .

Above, the matrix Z' in (6) is constructed such that $Z'_i = z'_i$ and $Z'_j = Z_j$ for all other $i \neq j$. The notation $z'_i \sim q_\delta(z_i, z'_i)$ denotes drawing z'_i from a symmetric distribution centered at z_i with $\delta > 0$ denoting a tuning parameter for the width, or *step size* of the proposal. Computing (6) involves only the prior for z_i and the (at most n) likelihood terms corresponding to dyads containing i —all other terms are equivalent for Z and Z' . For a fully observed network A , each full sweep updating Z thus requires $O(n^2)$ computations.

Like for random walk Metropolis, it is standard practice to tune δ using preliminary tuning runs to achieve a desired acceptance rate². The required value of δ typically shrinks as n grows, meaning that chains must be run much longer to achieve mixing when fitting larger networks. For example, Figure 6 in Appendix 6.3 demonstrates the decreasing relationship between the number of nodes and the tuned Metropolis within Gibbs step size δ for the variety of different synthetic networks considered in Section 4.2.

For large enough n , approximating the posterior using Metropolis within Gibbs thus also becomes intractable [Raftery et al., 2012]—the step-size is too small to efficiently explore the space given the complexity of computing the Metropolis-Hastings acceptance ratios. There have been multiple recent proposals that approximate the LPM likelihood [Raftery et al., 2012, Rastelli et al., 2018] to alleviate the computational burden of the accept-reject step. But as noted in the introduction, these approximations introduce non-vanishing bias in the subsequent inference.

Our goal in this article is to avoid such bias completely by developing an MCMC algorithm that outperforms Metropolis within Gibbs without sacrificing exactness of the sampler. To do so, we rely on a Monte Carlo algorithm known as Hamiltonian Monte Carlo (HMC). Recently, HMC has gained traction in the literature for fitting LPMs within large hierarchical models (e.g. Salter-Townshend and McCormick [2017] as implemented in Stan and Linderman et al. [2016] directly). However, we are the first (to our knowledge) to both develop a HMC algorithm that is specifically tooled for inference in LPMs, as well as the first to quantify their superior performance to other algorithms in the literature.

²Empirically, we have found that for LPMs, a Metropolis within Gibbs acceptance rate somewhere between 20 and 30 percent gives optimal results—this is consistent with related optimal scaling theory [Roberts et al., 2001]

2.3 Hamiltonian Monte Carlo

Hamiltonian Monte Carlo (HMC) is an auxiliary variable MCMC algorithm that uses the gradient of the log posterior to inform an efficient Markov proposal kernel. Inspired by Hamiltonian dynamics, HMC augments the posterior distribution with a “momentum” variable for each target parameter, framing the task of proposing the next state of the Markov chain as that of simulating Hamiltonian motion of an object along a high-dimensional surface.

An HMC chain consists of a sequence of snapshots of the object sliding along a high-dimensional surface (without friction). The object’s momentum is randomly refreshed each time a snapshot is taken, thus resulting in a sequence of stochastic draws. By using the negative log posterior as the energy function to inform its Hamiltonian motion, HMC provides larger step sizes that nevertheless maintain high Metropolis-Hastings acceptance rates. Moreover, these ratios have closed forms due to the properties of Hamiltonian dynamics (namely reversibility and volume preservation). The algorithm is thus efficient for exploring high-dimensional posteriors.

We now provide a description of HMC, placing emphasis on the components relevant to the development of our algorithm for the LPM. For more detailed reviews of the theory and practice of MCMC, Neal [2011] or Betancourt [2017] are fantastic references.

Consider a target density $p(Z)$ that is differentiable with respect to its real-valued parameters $Z \in \mathbb{R}^d$. HMC targets an augmented³ version of this density $p(Z, U) = p(Z)q(U)$ where $U \in \mathbb{R}^d$ is a vector of auxiliary momentum variables—each corresponding to an entry in Z . Let $q(U)$ be a zero mean multivariate Gaussian density with covariance matrix $M \in \mathbb{R}^{d \times d}$, and let $H(Z, U) = -\log(p(Z)) - \log(q(U))$. This function $H(Z, U)$ plays the role of energy in the Hamiltonian dynamics of HMC, with the covariance M (sometimes referred to as the *Mass matrix* [Neal, 2011] or *Euclidean metric* [Betancourt, 2017]) controlling the effect of the momentum on the dynamics.

³Note that because the density $p(Z, U)$ admits $p(Z)$ as a marginal, discarding the U ’s from a Markov chain targeting $p(Z, U)$ yields draws from $p(Z)$.

Hamiltonian motion over $H(Z, U)$ is governed by the following differential equations:

$$\frac{dZ_i}{dt} = \frac{\partial H(Z, U)}{\partial U_i} = (M^{-1}U)_i \quad (7)$$

$$\frac{dU_i}{dt} = \frac{-\partial H(Z, U)}{\partial Z_i} = \frac{\partial \log(p(Z))}{\partial Z_i}. \quad (8)$$

Here, $(M^{-1}U)_i$ denotes the i th coordinate in the vector $M^{-1}U$, and t represents the artificial “time” for which the Hamiltonian trajectory is computed. That is, the derivatives of Z and U with respect to t reflect the rate of change in these quantities along Hamiltonian trajectory. Starting at an initial state (Z^0, U^0) , HMC generates a Markov chain of snapshots $(Z^j, U^j)_{j \in \mathbb{N}}$ with stationary distribution $p(Z, U)$ by iterating between simulating Hamiltonian motion for a fixed amount of time $T > 0$, then refreshing the momentum according to its conditional distribution. The value of T is typically specified by the user to control the length of time between momentum updates.

Given (Z^j, U^j) , the next draw (Z^{j+1}, U^{j+1}) is obtained using the following steps

1. Gibbs update the momentum variables via Gibbs $U^{j'} \sim \text{MVN}(0, M)$.
2. Simulate Hamiltonian motion $(Z^j, U^{j'}) \rightarrow (Z^{j''}, U^{j''})$ for T time units.
3. Accept the move $(Z^{j+1}, U^{j+1}) = (Z^{j''}, -U^{j''})$ with probability

$$\min \left(\frac{p(Z^{j''}, U^{j''})}{p(Z^{j'}, U^{j'})}, 1 \right). \quad (9)$$

Otherwise reject the move, letting $(Z^{j+1}, U^{j+1}) = (Z^j, U^{j'})$.

The negation of $U^{j''}$ in Step 3 ensures the proposal is reversible⁴.

The performance of HMC as described above depends on two parameters chosen by the user: the mass matrix M and the amount of time T between momentum updates. Before discussing strategies for choosing these parameters, we must first address how to simulate Hamiltonian motion.

⁴In practice, the marginal distribution of Z (and not the joint distribution of Z, U) is the target of HMC, so this negation step can be omitted because it is immediately changed by subsequent Gibbs update of U [Neal, 2011].

If the Hamiltonian motion in Step 2 above were to be simulated exactly, the Metropolis-Hastings correction in Step 3 would be unnecessary because the ratio is exactly one [Neal, 2011]. This property is guaranteed by the conservation of energy in Hamiltonian motion—Step 2 simply moves along a density contour of the augmented distribution. Unfortunately, exact simulation of the Hamiltonian motion is not possible for most posterior densities that arise in Bayesian inference—there is no known analytic way to move along the contours.

In practice, simulation of the trajectory of Hamiltonian motion is typically carried out using approximate numerical integrators of the differential equations, the most popular of which is the *leapfrog integrator* [Neal, 2011] (sometimes referred to as the Stormer-Verlet integrator: e.g. [Chao et al., 2015]). The leapfrog integrator discretizes the Hamiltonian motion via alternating linear updates of U and Z until the trajectory of length T has been simulated. The following steps are iterated $L \in \mathbb{N}$ times:

$$U \leftarrow U - \frac{\epsilon}{2} \frac{\partial H}{\partial Z}(Z, U) \quad (10)$$

$$Z \leftarrow Z + \epsilon M^{-1} U \quad (11)$$

$$U \leftarrow U - \frac{\epsilon}{2} \frac{\partial H}{\partial Z}(Z, U) \quad (12)$$

Together, the user-specified parameters $\epsilon > 0$ (sometimes called the step-size) and $L \in \mathbb{N}$ (the number of steps) define leapfrog trajectory of length $T = L\epsilon$. Smaller values of ϵ provide more accurate approximations of the Hamiltonian motion (and thus the higher the Metropolis-Hastings acceptance rate), but also require correspondingly larger values of L —and thus more computation—to simulate a given trajectory length T . It is thus important to strike a balance between the two to obtain adequately high acceptance rates for reasonably correlated draws without wasting computational resources.

Choosing the user-specified parameters M and T for HMC via leapfrog amounts to choosing three parameters: the mass matrix M , the step size ϵ and the number of steps L . The original time parameter $T = L\epsilon$ is a byproduct of the choices of ϵ and L .

Like tuning the step-size for traditional Metropolis algorithms, standard practice for choosing ϵ and L is to conduct a series of preliminary tuning runs with various levels of the parameters, converging toward values that maximize the chain’s efficiency. Similarly, the

matrix M can also be chosen according to these tuning runs. A theoretically motivated heuristic [Betancourt, 2017] is to set M equal to an estimator of the precision matrix of the posterior, estimated from the empirical posterior covariance in the preliminary chains. In practice, the true precision matrix may be dense (and thus expensive to compute), meaning that a diagonal approximation [Carpenter et al., 2017] or a low-rank approximation [Bales et al., 2019] of the precision may also be a suitable choice. The former is implemented in the software package Stan.

Unfortunately, efficiently tuning all three of L , ϵ , and M can itself be a computationally burdensome because the three parameters are interdependent (the optimal choice of ϵ relies particularly heavily on the choice of M). Indeed, under the standard settings, it is typical for Stan to devote more time to adapting L , ϵ and M than running the final Markov chain. When the computational problem is already straining the computational budget at hand—such as in the case of large LPMs—these tuning costs can be prohibitive. We thus seek a simpler, more easily tunable algorithm that is specialized to large LPMs.

Before proceeding, it is worth noting that strategies exist for which L , ϵ and M are not necessarily held constant through all regions of the posterior. For instance, sophisticated algorithms exist for selecting L (e.g. the No-U-Turn sampler (NUTS [Hoffman and Gelman, 2014])), or M (e.g. Riemannian HMC Girolami and Calderhead [2011]) adaptively depending on the current state of the chain. However, these algorithms can be incredibly computationally intensive, as they can require many additional density, gradient, or Hessian evaluations. This is evident when we compare Stan and NUTS to our strategy in Section 4.2.

In the sequel, we derive an alternative HMC integration strategy that exploits the function form of the GLPM posterior for efficient exploration without costly tuning runs for L and M . Moreover, it locally adapts M to the link function parameter γ —providing a natural locally-adaptive choice of M that does not require computation of expensive Hessian calculations in Girolami and Calderhead [2011].

3 New Sampling Methodology

Our new MCMC algorithm for the GLPM is composed of three novel components: a split Hamiltonian Monte Carlo [Shahbaba et al., 2014] integrator to update the latent positions (Section 3.1), a Firefly Monte Carlo (FlyMC [Maclaurin and Adams, 2015]) auxiliary variable scheme to sub-sample non-edge dyads (Section 3.2), and Gibbs sampling strategies to update the parameters τ and γ^2 of the link probability function K (Section 3.3). We present each of these contributions in sequence.

3.1 Split Hamiltonian Monte Carlo

Though it is certainly the most popular for HMC, the leapfrog integrator is just one of many options for integrating Hamiltonian dynamics (e.g. Leimkuhler and Reich [2004], Chao et al. [2015], Mannseth et al. [2016]). Here, we consider an alternative called *split Hamiltonian Monte Carlo* [Shahbaba et al., 2014]. Split HMC is a variant on the leapfrog strategy that efficiently integrates Hamiltonian’s equations by leveraging a Gaussian component of the posterior. It works best when the Gaussian component is a good approximation of the posterior. As an added bonus, split HMC provides a natural and effective choice for the mass matrix M .

Note that the standard leapfrog update described in Section 2.3 is equivalent to decomposing the energy into three terms:

$$H(Z, U) = -\frac{1}{2} \log(p(Z)) - \log(q(U)) - \frac{1}{2} \log(p(Z)). \quad (13)$$

then cycling through isolated updates according (7) and (8) for each of the components individually. This “split” of the energy ensures that only one of Z or U is being updated at any given time, causing each isolated operation to be straightforward. In split Hamiltonian Monte Carlo, we consider a different split of the energy function, decomposing it to exploit partial analytic solutions of Hamiltonian equations.

Hamilton’s equations usually lack an analytic solution, but one of a few notable exceptions occurs when the energy is defined as the negative logarithm of a multivariate Gaussian density [Pakman and Paninski, 2014] (other exceptions include the univariate exponential

and uniform distributions [Bloem-Reddy and Cunningham, 2016]). For the Gaussian case, the motion and momentum updates can be simulated exactly along an ellipse (i.e. a contour of the Multivariate Gaussian distribution). Alone, this fact would have limited utility for Bayesian computation; exact algorithms for inference involving Gaussian posteriors are readily available. As part of an energy splitting strategy, however, these analytic solutions can be remarkably useful.

The split Hamiltonian integrator [Shahbaba et al., 2014] alternates between joint position momentum updates based on the analytical solution of the Gaussian component of the posterior and updates to the momentum to correct for the remaining portion of the posterior. When the exact part is a good approximation for the entire posterior, this allows for a coarser ϵ to maintain a high acceptance rate.

To make things more concrete, we now present the decomposition of the GLPM posterior into its Gaussian and non-Gaussian components. Specifically, the likelihood of the edges, the prior density, and the momentum forming the Gaussian component, and the likelihood of non-edges forms the remainder.

Recall the LPM posterior's functional form as provided in (5). Treating the τ and γ^2 as known, (5) takes the form

$$\mathbb{P}(Z|A, \tau, \gamma^2) = \prod_{\{i,j\} \in E_A} \tau_{x_{ij}} \exp \left(-\frac{1}{2} \sum_{\ell=1}^d Z_{\ell}^T \left(\Omega + \frac{1}{\gamma^2} L^A \right) Z_{\ell} \right) \prod_{(i,j) \notin E_A} \left(1 - \tau_{x_{ij}} \exp \left(-\frac{\|z_i - z_j\|^2}{2\gamma^2} \right) \right) \quad (14)$$

where L^A denotes the Laplacian of A . This posterior can thus be decomposed into two components $\mathbb{P}(Z|A, \tau, \gamma^2) = \mathbb{P}_1(Z|A, \tau, \gamma^2) \mathbb{P}_0(Z|A, \tau, \gamma^2)$ where

$$\mathbb{P}_1(Z|A, \tau, \gamma^2) = \left(\prod_{\{i,j\} \in E_A} \tau_{x_{ij}} \right) \exp \left(-\frac{1}{2} \sum_{\ell=1}^d Z_{\ell}^T \left(\Omega + \frac{1}{\gamma^2} L^A \right) Z_{\ell} \right) \quad (15)$$

corresponds to the contribution of the prior and likelihood of the observed edges and

$$\mathbb{P}_0(Z|A, \tau, \gamma^2) = \prod_{ij \notin E_A} \left(1 - \tau_{x_{ij}} \exp \left(-\frac{1}{2\gamma^2} \|z_i - z_j\|^2 \right) \right) \quad (16)$$

corresponds to the contribution to the likelihood of the non-edges.

Using the shorthand

$$\Sigma = \left(\Omega + \frac{1}{\gamma^2} L^A \right), \quad (17)$$

we can now split the corresponding energy as

$$H(Z, U) = \left[-\frac{1}{2} \log(\mathbb{P}_0(Z|A, \tau, \gamma^2)) \right] + \left[\frac{1}{2} \sum_{\ell=1}^d (Z_{\cdot\ell}^T \Sigma Z_{\cdot\ell} + U_{\cdot\ell}^T M^{-1} U_{\cdot\ell}) \right] - \left[\frac{1}{2} \log(\mathbb{P}_0(Z|A, \tau, \gamma^2)) \right], \quad (18)$$

ignoring additive constants. The center term in this split is Gaussian.

In the above, we have departed from the typical notation in our definition of the mass matrix M and momentum variables U . In standard presentations of HMC (including our presentation of HMC in Section 2.3), the target parameters and momentum variables are naturally represented as vectors. For a LPM, the parameters Z are more suitably represented a $n \times d$ matrix. We have thus chosen to also represent the momentum variables U as a $n \times d$ matrix. Since there are $n \times d$ momentum variables, the standard notation/definition of the mass matrix would require that $M \in \mathbb{R}^{nd \times nd}$. We have opted to instead define the full mass matrix block diagonally, using d repetitions of the same matrix $M \in \mathbb{R}^{n \times n}$. This choice facilitates the more compact representation in (18) without altering the validity of the algorithm.

On top of being notationally and computationally convenient, the use of an identical mass matrix across all dimensions is justified by symmetry in the target posterior—the marginal distribution of each column of Z is the same [Shortreed et al., 2006].

The above decomposition thus suggests a natural choice of M . Recall from Section 2.3 that the precision matrix of the posterior is an efficient choice for M . Accordingly, we suggest that Σ is a reasonable choice for M , as it should be a good approximation of the posterior precision matrix provided that \mathbb{P}_0 is a good approximation of the full posterior. Moreover, the choice $M = \Sigma$ is also particularly amenable to simulating the split HMC trajectories because it leads to arithmetic cancellations that simplify computation. Finally, the mass matrix M depends on the parameter γ^2 —when combined with a Monte Carlo strategy for inferring γ^2 (such as the we present in Section 3.3), setting $M = \Sigma$ allows for the mass matrix to evolve adaptively with the state of γ^2 in the chain.

The following is a complete recipe for split HMC for LPMs, using the block diagonal mass matrix we have just defined. Note that the intermediate variable $V \in \mathbb{R}^{n \times d}$ introduced in Step 2 is a change of variable for efficiently parametrizing the contour of the multivariate Gaussian, and Step 4 inverts the change of variable to recover U . For more details on the exact simulation of HMC for Multivariate Gaussians, see Pakman and Paninski [2014].

Suppose that A denotes an observed adjacency matrix, $\tau \in [0, 1]^C$ and $\gamma^2 > 0$ denote the values of the parameters of the Gaussian link function, and $\epsilon > 0$, $L \in \mathbb{N}$ and Σ (as defined in (17)) denote the user-specified tuning parameters for split HMC. Given (Z^j, U^j) , the next split HMC draw (Z^{j+1}, U^{j+1}) is obtained via the following steps:

1. Gibbs update the momentum variables via Gibbs $U^{j'} \sim \text{MVN}(0, \Sigma)$.
2. Define intermediate variables $V^{j'} = \Sigma^{-1}U^{j'}$ and $Z^{j''} = Z^j$.
3. Integrate Hamiltonian motion $(Z^j, U^{j'}) \rightarrow (Z^{j''}, U^{j''})$ for $T = L\epsilon$ time units

by iterating the following updates L times:

$$V^{j'} \leftarrow V^{j'} + \frac{\epsilon}{2} \Sigma^{-1} \frac{\partial \log(\mathbb{P}_0(Z|A, \tau, \gamma^2))}{\partial Z} (Z^{j''}) \quad (19)$$

$$(Z^{j''}, V^{j'}) \leftarrow \left(\sin(\epsilon)V^{j'} + \cos(\epsilon)Z^{j''}, \cos(\epsilon)V^{j'} - \sin(\epsilon)Z^{j''} \right) \quad (20)$$

$$V^{j'} \leftarrow V^{j'} + \frac{\epsilon}{2} \Sigma^{-1} \frac{\partial \log(\mathbb{P}_0(Z|A, \tau, \gamma^2))}{\partial Z} (Z^{j''}) \quad (21)$$

4. Let $U^{j''} = \Sigma V^{j'}$.
5. Accept the move $(Z^{j+1}, U^{j+1}) = (Z^{j''}, -U^{j''})$ with probability

$$\min \left(\frac{\mathbb{P}(Z^{j''}|A, \tau, \gamma^2)}{\mathbb{P}(Z^j|A, \tau, \gamma^2)} \exp \left(\frac{1}{2} \sum_{\ell=1}^d (U'_{\ell} - U''_{\ell})^T \Sigma^{-1} (U'_{\ell} - U''_{\ell}) \right), 1 \right). \quad (22)$$

Otherwise, the move is rejected and $(Z^{j+1}, U^{j+1}) = (Z^j, U^{j'})$.

In Step 2 above, the gradient functions return $n \times d$ matrices defined by

$$\left(\frac{\partial \log(\mathbb{P}_0(Z|A, \tau, \gamma^2))}{\partial Z} (Z) \right)_{ik} = \frac{\partial \log(\mathbb{P}_0(Z|A, \tau, \gamma^2))}{\partial Z_{ik}} \quad (23)$$

$$= \sum_{j:ij \notin E_A} \frac{(Z_{ik} - Z_{jk})}{\gamma^2} \frac{\tau_{x_{ij}} \exp\left(-\frac{\|z_i - z_j\|^2}{2\gamma^2}\right)}{1 - \tau_{x_{ij}} \exp\left(-\frac{\|z_i - z_j\|^2}{2\gamma^2}\right)}. \quad (24)$$

Computing the gradients in (24) and the acceptance ratio in Steps 2 and 4 represent the main computational bottlenecks of our split HMC algorithm for LPMs, as they both require an operation be performed for each non-edge. Note that large sparse networks possess many non-edges. For such networks, it is especially important that we compute the gradients as efficiently as possible because the optimal value of L may be large. Motivated by this computational bottleneck, we now develop an exact subsampling strategy to reduce the number of non-edges that must be considered for each gradient computation.

3.2 Firefly Sampling of Non-Edges

Recall from Section 3.1 that the obstacle preventing exact simulation of the Hamiltonian motion is the presence of the non-edge terms in the likelihood. Moreover, the computational bottleneck for running the proposed split HMC algorithm is the density and gradient operations that involved the non-edges. Thus, it could be beneficial to eliminate some of non-edge terms of the model likelihood at each iteration of split HMC. Here, we propose such a strategy.

Consider the following data augmentation scheme inspired by the Firefly Monte Carlo (FlyMC [MacLaurin and Adams, 2015]). For each $i, j \in [n]^2$, we define auxiliary independent binary random variables θ_{ij} such that $\mathbb{P}(\theta_{ij} = 1 | \tau_{x_{ij}}) = \tau_{x_{ij}}$. Using these auxiliary variables, we can re-express the edge probabilities as

$$\mathbb{P}(A_{ij} = 1 | \theta_{ij} = 1, \tau_{x_{ij}}, \gamma^2) = \exp\left(-\frac{1}{2\gamma^2} \|z_i - z_j\|^2\right) \quad (25)$$

$$\mathbb{P}(A_{ij} = 1 | \theta_{ij} = 0, \tau_{x_{ij}}, \gamma^2) = 0, \quad (26)$$

while maintaining the same marginal likelihood. Now,

$$\mathbb{P}(\theta_{ij} = 0 | A_{ij} = 0, Z, \tau_{x_{ij}}, \gamma^2) = \frac{1 - \tau_{x_{ij}}}{1 - \tau_{x_{ij}} \exp\left(-\frac{1}{2\gamma^2} \|z_i - z_j\|^2\right)}, \quad (27)$$

$$\mathbb{P}(\theta_{ij} = 0 | A_{ij} = 1, Z, \tau_{x_{ij}}, \gamma^2) = 0. \quad (28)$$

Note that for all $(i, j) \in E_A$, $\theta_{ij} = 1$ must hold. Thus,

$$\mathbb{P}(Z | A, \theta, \tau, \gamma^2) = \mathbb{P}_1(Z | A, \tau, \gamma^2) \prod_{ij: \theta_{ij}=1, A_{ij}=0} \left(1 - \exp\left(-\frac{1}{2\gamma^2} \|z_i - z_j\|^2\right)\right), \quad (29)$$

meaning that

$$\mathbb{P}_0^*(Z|A, \theta, \tau, \gamma^2) = \prod_{ij: \theta_{ij}=1, A_{ij}=0} \left(1 - \exp \left(-\frac{1}{2\gamma^2} \|z_i - z_j\|^2 \right) \right) \quad (30)$$

can replace $\mathbb{P}_0(Z|A, \tau, \gamma^2)$ in Split HMC once the θ variables are instantiated. If many of the θ_{ij} are 0, computing $\mathbb{P}_0(Z|A, \tau, \gamma^2)$ —and its gradients—is far cheaper than computing the marginal $\mathbb{P}_0(Z|A, \tau, \gamma^2)$ analogs. Thus, combining the above with split HMC can represent a major computational improvement, provided that we can instantiate and update the θ_{ij} values efficiently.

To do so, we propose a Metropolis-Hastings step using proposal $q(\theta_{ij} = 1) = \tau_{ij}$. Let $\text{MH}(\theta_{ij} = 0 \rightarrow \theta_{ij} = 1)$ denote the Metropolis-Hastings ratio associated with a proposed move from $\theta_{ij} = 0$ to $\theta_{ij} = 1$, and let $\text{MH}(\theta_{ij} = 1 \rightarrow \theta_{ij} = 0)$ denote the Metropolis-Hastings ratio associated with a proposed move from $\theta_{ij} = 1$ to $\theta_{ij} = 0$. The values of these ratios are given by

$$\text{MH}(\theta_{ij} = 0 \rightarrow \theta_{ij} = 1) = \left(1 - \exp \left(-\frac{1}{2\gamma_{ij}^2} \|z_i - z_j\|^2 \right) \right), \quad (31)$$

$$\text{MH}(\theta_{ij} = 1 \rightarrow \theta_{ij} = 0) = \frac{1}{1 - \exp \left(-\frac{1}{2\gamma_{ij}^2} \|z_i - z_j\|^2 \right)} > 1. \quad (32)$$

Thus, out of the four possible moves $0 \rightarrow 0$, $0 \rightarrow 1$, $1 \rightarrow 0$, $1 \rightarrow 1$, the accept reject step need only be performed for $0 \rightarrow 1$. Therefore, this strategy is more computationally efficient than updating each θ_{ij} according to its full conditional using a Gibbs update.

Going forward, we refer to the parameter augmentation and update strategy described above as FlyMC. The reduction in computational cost of evaluating the posterior density and gradients under FlyMC is most prevalent when most of the θ_{ij} are 0. Because the $\mathbb{P}(\theta_{ij} = 0 | \tau_{x_{ij}}) = 1 - \tau_{x_{ij}}$, the computational gains from FlyMC are thus largest when $\tau_{x_{ij}}$ is small. On the other hand, when $\tau_{x_{ij}}$ are relatively large (close to 1), most values of the θ_{ij} will be one, meaning the computational improvements in evaluating the gradient may not justify the computational expense of instantiating and updating the θ variables. In the extreme case of $\tau_{x_{ij}} = 1$, no subsampling will occur at all, so FlyMC should not be included.

For sparse networks, however, $\tau_{x_{ij}}$ may be very small for some values of x_{ij} , leading to substantial computational gains. In addition to providing a computational speed-up, the new FlyMC posterior facilitates the inference of τ via Gibbs steps. We now discuss MCMC updates for τ and γ^2 in Section 3.3.

3.3 Bayesian Inference of the Parameters of the Link Function

Thus far, our posterior computation strategy for Z has held τ and γ^2 —the parameters of the link function—at fixed values. In most applications, τ and γ^2 are unknown—they need to be inferred along with Z . As we noted in Section 2.2, τ may even be the primary inferential target when the main scientific question involves measuring the effect of a covariate. For these reasons, it is important that our posterior computation strategy be able to compute the full joint posterior of τ , γ^2 , and Z . Here, we describe efficient Gibbs updates for both τ (Section 3.3.1) and γ^2 (Section 3.3.2) that can be alternated with our split HMC + FlyMC strategy (Sections 3.1 and 3.2) for updating Z to define a complete MCMC algorithm.

Before proceeding, it is worth making a couple of notes. The updates we describe here apply to specific families of priors on τ and γ^2 : independent Beta priors being used for each entry in τ and an inverse Gamma prior γ^2 . Moreover, the update for τ is only applicable in conjunction with the FlyMC strategy outlined in Section 3.2. If FlyMC is not used (and thus the θ are not available), we recommend a simple random walk Metropolis-Hastings update for τ instead. Finally, our update strategy for γ^2 depends on a re-parameterization of the model that shifts direct inference of γ^2 in the link function to inference of a constant multiple on the variance Ω of the latent positions Z . This facilitates a conversion to a centered parameterization [Papaspiliopoulos et al., 2007] of Z , allowing a Gibbs update where one was previously intractable. This Gibbs update of γ^2 is applicable whether or not FlyMC is used.

3.3.1 Updating τ given Z, θ, γ^2

Suppose that each of the C entries in the vector τ are assigned independent priors such that $\tau_c \sim \text{Beta}(\alpha_c, \beta_c)$ for $c \in [C]$, $\alpha, \beta \in \mathbb{R}_+^C$. Then, if the FlyMC strategy outlined in Section 3.2

is used, each τ_c can be Gibbs updated according to its conditional posterior distribution given the FlyMC variables θ and the covariates x . Indeed, this posterior distribution is actually conjugate to the Beta prior because inferring $\tau_c|\theta, x$ for $c \in [C]$ is equivalent to inferring the probability parameter of a sequence of Bernoulli trials (specifically the θ_{ij} for which $x_{ij} = c$). Thus,

$$\tau_c \mid \theta, x \sim \text{Beta}(\alpha_c + \Theta_c^1, \beta_c + \Theta_c^0) \quad (33)$$

for each $c \in [C]$, where $\Theta^0, \Theta^1 \in (\{0\} \cup \mathbb{N})^C$ are defined according to

$$\Theta_c^0 = |\{\{i, j\} \in [n]^2 : \theta_{ij} = 1 \text{ and } x_{ij} = c\}| \quad (34)$$

$$\Theta_c^1 = |\{\{i, j\} \in [n]^2 : \theta_{ij} = 0 \text{ and } x_{ij} = c\}|. \quad (35)$$

This update can be efficiently updated by keeping track of the values of Θ^0 and Θ^1 when performing the FlyMC updates.

3.3.2 Updating γ^2 given Z, τ, θ

Suppose we place an $\text{InverseGamma}(a, b)$ prior on γ^2 , where $a, b > 0$. Then, the posterior density of $\gamma^2|A, Z, \theta, \tau, x$ is proportional to

$$p(\gamma^2 \mid A, Z, \theta, \tau, x) = \text{IG}(\gamma^2|a, b) \exp \left(-\frac{1}{2\gamma^2} \sum_{\ell=1}^d Z_{\cdot\ell}^T L^A Z_{\cdot\ell} \right) \prod_{ij: \theta_{ij}=1, A_{ij}=0} \left(1 - \exp \left(-\frac{1}{2\gamma^2} \|z_i - z_j\|^2 \right) \right) \quad (36)$$

where $\text{IG}(\gamma^2|a, b)$ denotes the probability density function of the $\text{InverseGamma}(a, b)$ distribution evaluated at γ^2 . This density provides no closed-form Gibbs update and is expensive to evaluate so working directly with it would be cumbersome as part of an MCMC strategy.

However, we can remedy this situation via a re-parameterization. Recall that Z has a Gaussian prior defined by $Z_{\cdot\ell} \sim N(0, \Omega)$ for $\ell \in [d]$. Thus, the re-parameterized random variable $Z^* = \gamma^{-1}Z$ has a conditionally multivariate Gaussian prior defined by $Z_{\cdot\ell}^* \mid \gamma^2 \sim$

$N(0, \gamma^{-1}\Omega)$ for $\ell \in [d]$. The conditional distribution of γ^2 given A, Z^*, θ, τ, x is given by

$$p(\gamma^2 | A, Z^*, \theta, \tau, x) = \text{IG}(\gamma^2 | a, b) \exp \left(-\frac{\gamma^2}{2} \sum_{\ell=1}^d (Z_{\cdot\ell}^*)^T \Omega^{-1} Z_{\cdot\ell}^* \right) \quad (37)$$

$$= \text{IG} \left(\gamma^2 | a + \frac{nd}{2}, b + \frac{1}{2} \sum_{\ell=1}^d (Z_{\cdot\ell}^*)^T \Omega^{-1} Z_{\cdot\ell}^* \right). \quad (38)$$

Therefore, by conditioning on Z^* instead of Z , the posterior dependence of γ^2 on θ and A have been removed—it depends solely on Z^* . Moreover, the prior on γ^2 is now conjugate, and can be updated via a simple Gibbs update.

Fortunately, this re-parameterization and the corresponding Gibbs update can be easily incorporated with the updates of Z , θ , and τ described in Sections 3.1, Section 3.2, and Section 3.3.1, respectively. Doing so requires just a small re-tooling of the model/notation. Instead of viewing the Gaussian LPM as having latent positions Z with prior $Z_{\cdot\ell} \sim N(0, \Omega)$ and a two parameter link function defined in (4), we can re-express the Gaussian LPM with Z^* taking the role of the latent positions, γ^2 being a hyperparameter of their prior $Z_{\cdot\ell}^* \sim N(0, \gamma^{-1}\Omega)$, and the edges generated according to a one parameter link function defined by

$$K(\|z_i^* - z_j^*\|, x_{ij}) = \tau_{x_{ij}} \exp \left(-\frac{1}{2} \|z_i^* - z_j^*\|^2 \right). \quad (39)$$

Because the updates of Z (Section 3.1), θ (Section 3.2), and τ (Section 3.3.1) treated γ^2 as fixed, they are equally applicable after this re-parametrization—we just fix the γ^2 in the link function at 1, and have Z^* play the role of Z (with a new hyperparameter γ^2 on the prior). After performing MCMC sampling this re-parametrized setting, one can recover the original parameterization of Z by simply undoing the change-of-variable transformation.

Thus, we have now defined a full MCMC strategy for posterior computation of Z, τ, γ^2 that also introduces and updates auxiliary FlyMC variables θ . Each sweep of the chain iterates through a split HMC update of Z , a Metropolis update of each θ , a Gibbs update for each entry in τ , and a Gibbs update of γ^2 . Alternatively, if FlyMC is not incorporated, posterior computation of Z , τ , and γ^2 can be performed by alternating the split HMC update of Z , a Metropolis update of each entry in τ , then a Gibbs update of γ^2 . For

completeness, the functional form of the posterior being computed in both the split HMC and split HMC + FlyMC algorithms is outlined in Section 6.2 of the Appendix.

4 Empirical Studies

To explore and understand the relative strengths and weaknesses of our new posterior inference algorithm for GLPMs, we conduct two empirical studies. Study 1 (Section 4.2) consists of a “bake-off” between various inference algorithms, comparing the efficiency of our method to that of plausible competitors from in literature. These comparisons span a variety of synthetically generated networks of different sizes and sparsity levels. Study 2 (Section 4.3) is a real data example, demonstrating efficiency of split HMC and split HMC + FlyMC compared to traditional Metropolis within Gibbs for modeling information-sharing among elementary school teachers and staff in a school district. It considers multiple model set-ups, including the use of use categorical covariates and longitudinal network data. Details of the computational software and hardware used to run the experiments is provided in Section 6.1 of the Appendix.

Before delving into Studies 1 and 2, Section 4.1 motivates and describes our metric for comparing the relative efficiency of various Monte Carlo algorithms for LPMs.

4.1 Measuring relative efficiency of MCMC Algorithm for LPMs

There are two principal criteria by which to judge the efficiency of a Markov chain for approximating a posterior distribution.

1. How efficiently does the MCMC sequence approximate the posterior expectation of a desired function of the parameters?
2. What is the computational expense of generating this chain?

Simple metrics exist for gauging each of these criteria, which we describe below.

For criterion 1, it is well-known that that mean estimates stemming from a geometrically ergodic [Roberts et al., 1997] Markov chain are subject to a Markov chain central limit

theorem (CLT) [Tierney, 1994]. Analogous to the standard (independent samples) central limit theorem, for which the variance of the estimator is inversely proportional to the raw sample size, the variance in the Markov chain CLT is inversely proportional to the *Effective sample size* [Kass et al., 1998, Ripley, 2009].

Letting $\theta^1, \theta^2, \dots, \theta^N$ denote N draws from a Markov chain and f denote an arbitrary function, the effective sample size ESS_f for estimating the expectation of $f(\theta)$ is defined as

$$ESS_f(\theta^1, \dots, \theta^N) = \frac{N}{1 + 2 \sum_{t=1}^{\infty} \rho_{t,f}} \quad (40)$$

where

$$\rho_{t,f} = \frac{\int f(\theta^{i+t}) f(\theta^i) p(\theta^i) d\theta^i}{\int f(\theta^i)^2 p(\theta^i) d\theta^i} \quad (41)$$

denotes the t -lag autocorrelation of the function $f(\theta)$ in the Markov chain.

The effective sample size thus takes into account all possible lags of autocorrelations, recognizing that highly autocorrelated chains represent fewer bits of independent information than an uncorrelated analog. In practice, estimating the effective sample size of a chain is done by estimating the autocorrelations. For our purposes, we use the effective sample size estimator implemented in the R package `coda` [Plummer et al., 2006].

We should note that we have not formally proved that our proposed HMC + FlyMC algorithm (as well the other algorithms considered here) produces a geometrically ergodic Markov chain (see Mangoubi and Smith [2017], Livingstone et al. [2019], Mangoubi and Smith [2019] for recent progress on related problems). However, the effective sample size remains an intuitive metric for the efficiency of a Markov chain approximation, due to its penalization of autocorrelations. Moreover, conservative confidence intervals based on the effective sample size can still be constructed even when geometric ergodicity does not necessarily hold Rosenthal [2017]. For this reason, we feel it is still a suitable metric to use when comparing chains.

To assess criterion 2 (the computational expense of generating a chain), we simply measure the runtime⁵ of the algorithm. Although there is opportunity for parallelization

⁵None of the algorithms we consider here are memory-intensive. If any were, it might also make sense to report the memory requirements.

in some of the algorithms (e.g. simultaneous updating of FlyMC variables), we do not take advantage of such opportunities—all our implementations perform the various steps in series.

Overall, both criterion 1 and criterion 2 should be considered simultaneously when judging the efficiency of a Markov chain—a fast MCMC algorithm is not necessarily accurate, and an accurate MCMC algorithm is not necessarily fast. The most popular metric for combining these criteria is the effective sample size per second [Gamerman and Lopes, 2006], defined by

$$\text{ESS per second} = \frac{\text{ESS}_f(\theta^1, \dots, \theta^N)}{\text{time (in seconds) taken to compute the chain } \theta^1, \dots, \theta^N}, \quad (42)$$

sometimes referred to as Markov chain efficiency [de Valpine, 2018]. This metric provides a straightforward way to compare the performance of two MCMC algorithms. If one MCMC algorithm produces twice as many effective samples per second as another, that means it is twice as efficient, obtaining an equally accurate approximation of a desired posterior expectation in roughly half the time. This begs the question—what posterior expectation do we desire?

Typically, the posterior mean of the various parameters is the natural choice [Carpenter et al., 2017]. However, for the LPM, the posterior mean of each latent positions is inappropriate. Due to the invariance of the likelihood under isometric transformations (e.g. rotations and reflections [Shortreed et al., 2006]), all latent positions are guaranteed to have posterior mean of 0. If our target were the posterior means of the positions, MCMC would be unnecessary.

A reasonable target should instead be well-identified in the model, such as the probabilities of edges between the nodes. These values depend both on the latent positions and the parameters of the link function. However, there are $n(n - 1)/2$ such probabilities in total. For large networks, computing the effective sample size for all of them is computationally burdensome. Moreover, many of these expected probabilities will be very close to 0 in sparse networks, creating numerical underflow problems in practice.

To avoid having to compute the Markov efficiency for all $n(n - 1)/2$ unique pairs in $[n]^2$, we instead consider a uniformly random subset of 500 dyads (sampled without replacement)

for each of our empirical studies in Sections 4.2 and 4.3. Subsampling drastically reduces the amount of computation required while still providing a summary of how well the chain is mixing for all nodes. To avoid the underflow problems associated with estimating the raw probabilities, we calculate the effective sample size of estimating the log probabilities instead. That is, for a given $i, j \in [n]^2$, we consider

$$f(Z, \gamma, \tau, X) = \log(\tau_{x_{ij}}) - \frac{\|z_i - z_j\|^2}{2}. \quad (43)$$

as the function for which we calculate the posterior expectation. These functions are much more numerically tractable than the raw probabilities, whilst preserving strong ties with other quantities of interest (i.e. the distance between nodes and the density parameter τ).

Finally, we can now bring all of this together to define an interpretable quantity for reporting the relative efficiency of MCMC algorithms. Metropolis within Gibbs is currently the most popular MCMC algorithm for posterior computation of LPMs, making it the natural choice for the baseline against which to compare other algorithms in our empirical studies (Sections 4.2 and 4.3). Accordingly, we report each algorithm's efficiency relative to Metropolis within Gibbs for each subsampled dyad. That is, for a chain $\theta^1, \dots, \theta^N$, we calculate

$$\frac{\text{ESS}_f(\theta^1, \dots, \theta^N)}{\text{ESS}_f(\theta_m^1, \dots, \theta_m^N)} \times \frac{\text{time (in seconds) taken to compute the chain } \theta_m^1, \dots, \theta_m^N}{\text{time (in seconds) taken to compute the chain } \theta^1, \dots, \theta^N} \quad (44)$$

for each dyad, where $\theta_m^1, \dots, \theta_m^N$ denotes draws according to a well-tuned Metropolis within Gibbs algorithm exploring the same posterior.

4.2 Study 1: Synthetic Data

In this empirical study, we investigate the efficiency of split HMC (Section 3.1) and split HMC + FlyMC (Sections 3.1 and 3.2) compared to nine other exact MCMC algorithms from the literature. We are particularly interested in efficiently fitting LPMs to the large, sparse networks that have become increasingly common in modern applications, so we have toolled the study's design to showcase how the algorithms perform as the networks become larger and more sparse.

Our investigation involves fitting Gaussian LPMs to 16 different synthetically generated networks. These networks—stochastically generated according to a GLPMs with pre-specified values of τ , γ^2 , and Ω —demonstrate a variety of different sizes and sparsity. Specifically, they represent a full factorial design on the combinations of settings of the parameters $\tau \in \{0.2, 0.8\}$, $\gamma^2 \in \{0.2, 1.0\}$, and the number of nodes $n \in \{50, 100, 200, 500\}$. To generate each of these $2 \times 2 \times 4 = 16$ networks, the latent positions of the nodes are drawn independently from a two-dimensional isotropic Gaussian (i.e. $\Omega = I_n$) prior, and the edges were generated according to the link function with the designated τ, γ parameters. We do not include any observed covariates in this study (i.e. $C = 1$ for $\tau \in [0, 1]$).

Integrating the link probability function K in (4) with respect to the isotropic Gaussian prior on Z indicates that the expected probability of an edge between any two nodes i and j in the synthetically generated networks is given by

$$\mathbb{E}(A_{ij}) = \tau (1 + 2\gamma^{-2})^{-1}. \quad (45)$$

Thus, the parameter configurations described above exhibit a range of sparsity levels: For the $\tau = 0.2, \gamma^2 = 0.2$ networks, roughly 3 percent of dyads have edges, 10 percent of dyads have edges in the $\tau = 0.2, \gamma^2 = 1.0$ networks, 13 percent of dyads have edges in the $\tau = 0.8, \gamma^2 = 0.2$ networks, and 40 percent of dyads have edges in the $\tau = 0.8, \gamma^2 = 1.0$ networks. Though the $\tau = 0.8, \gamma^2 = 0.2$ and $\tau = 0.2, \gamma^2 = 1.0$ configurations correspond to similar edge counts (and thus sparsity levels), sparsity driven by small τ has a different structure than sparsity driven by γ^2 , so it is worthwhile investigating both.

For each of the 16 synthetically generated networks, we use (44) from Section 4.1 to compare the relative performance of 11 different MCMC algorithms. These algorithms primarily vary along two criteria: the proposal used to update Z , and whether or not FlyMC (Section 3.2) is used to subsample the non-edges. We consider five different strategies for updating Z : Metropolis within Gibbs (Section 2.2), elliptical slice sampling [Murray et al., 2010], elliptical slice sampling within Gibbs [Hahn et al., 2019], split HMC (Section 3.1) with $T \approx 2$, and an alternative implementation of Split HMC that uses NUTS [Hoffman and Gelman, 2014] to adaptively choose the integration time T . For each of these five strategies for updating Z , we consider both a standard implementation and FlyMC implementation,

amounting to ten different algorithms. Finally, we include HMC as implemented Stan (version 2.18.2 [Carpenter et al., 2017]) as an additional competitor algorithm, bringing the total number of algorithms to 11. Because Stan does not support discrete latent variables, a FlyMC version of Stan is not possible.

We included these algorithms for the following reasons: Metropolis within Gibbs is a baseline, as mentioned above. Both of the elliptical slice sampling algorithms were included as competitors because they represent alternative ways to exploit a Gaussian component in the posterior. The NUTS version of Split HMC was included to investigate whether extra computation cost of adaptively setting the integration time in HMC is worth it for LPMs. Stan was included to ensure our methods represented a worthwhile improvement over out-of-the-box general software.

In addition to inferring Z , all 11 algorithms are tooled to infer τ and γ^2 as well, using a standard uniform prior on τ and inverse gamma (IG(1,1)) prior on γ^2 . In Stan, all parameters (Z , γ^2 , and τ) are updated as part of a single HMC update. For the five FlyMC algorithms, we alternate between updates of Z as prescribed above, updates of the FlyMC variables θ according to the Metropolis strategy outlined in Section 3.2, updates of τ according to the Gibbs strategy outlined in Section 3.3.1, and an update of γ^2 to the Gibbs strategy outlined in Section 3.3.2. For the five remaining standard algorithms, we alternate between updates of Z as prescribed above, τ using a random walk Metropolis algorithm, and γ^2 to the Gibbs strategy outlined in Section 3.3.2.

Where appropriate, we tuned the parameters of the algorithms to promote efficient computation. Stan has a sophisticated (and computationally intensive) tuning strategy for choosing its step size ϵ along with a mass matrix M . For details, see Carpenter et al. [2017]. For all of the non-Stan algorithms, we used a light tuning strategy based on a sequence of short (100 iteration) preliminary runs to iteratively select reasonable values for the parameters. For the updates of Z , the Metropolis and Metropolis + FlyMC step sizes were chosen to target an acceptance rate in the range $[0.2, 0.3]$. For the split HMC and split HMC + FlyMC algorithms, the value of ϵ was determined by targeting an acceptance rate within $[0.8, 0.85]$. The value of L was chosen simultaneously to ensure $T = L\epsilon \approx 2$.

We have found through a wide array of preliminary experiments that these values tend to give results that are close to optimal without taking too much tuning time. For the NUTS algorithms, the value of ϵ chosen for the analogous split HMC algorithm was used. The elliptical slice algorithms have no tuning parameters. The step-size for the Metropolis τ updates was also chosen based on short preliminary runs, targeting an acceptance rate in the range $[0.2, 0.3]$. The step sizes used to update Z for split HMC, split HMC + FlyMC, Metropolis within Gibbs, and Metropolis within Gibbs + FlyMC are provided in Figure 6 in Section 6.3 of the Appendix.

For each of the 16 synthetic networks, we performed a single run of each algorithm for 10000 iterations (aside from Stan which we ran for just 2000 iterations due to its much longer runtime⁶). Each algorithm was initialized identically, using the maximum likelihood estimate of Z and the true values of τ and γ^2 as starting points. Figures 1 and 2 illustrate the relative efficiency of the eleven MCMC algorithms used to compute the posterior for the 16 different networks, with Figure 1 showing the standard implementations and Figure 2 showing the FlyMC implementations. For each posterior inference algorithm applied to each network, we calculated the Markov chain efficiency described in Section 4.1 for a random subset of 500 dyads in the network. To facilitate comparison between algorithms and parameter settings, we then determined the ratio in (44) for each algorithm and dyad to compare it to the Metropolis within Gibbs baseline. Figures 1 and 2 report the medians (across all edges) of these ratios for each algorithm and parameter setting. They are ordered according to the number of nodes to demonstrate how the relatively efficiency changes as the number of nodes increases.

The results shown in Figure 1 and Figure 2 demonstrate several phenomena. The first thing to note is that Split HMC and and Split HMC + FlyMC are the standout performers across all networks considered. Split HMC clearly outperforms Metropolis within Gibbs for all networks, and Split HMC + FlyMC clearly outperforms Metropolis within Gibbs for all networks except the 50 and 100 node networks in the sparsest regime. Notably, both implementations of Split HMC with $T \approx 2$ outperform their NUTS counterparts and Stan,

⁶The use effective sample size per second as our metric means that Stan is not penalized for running for fewer iterations

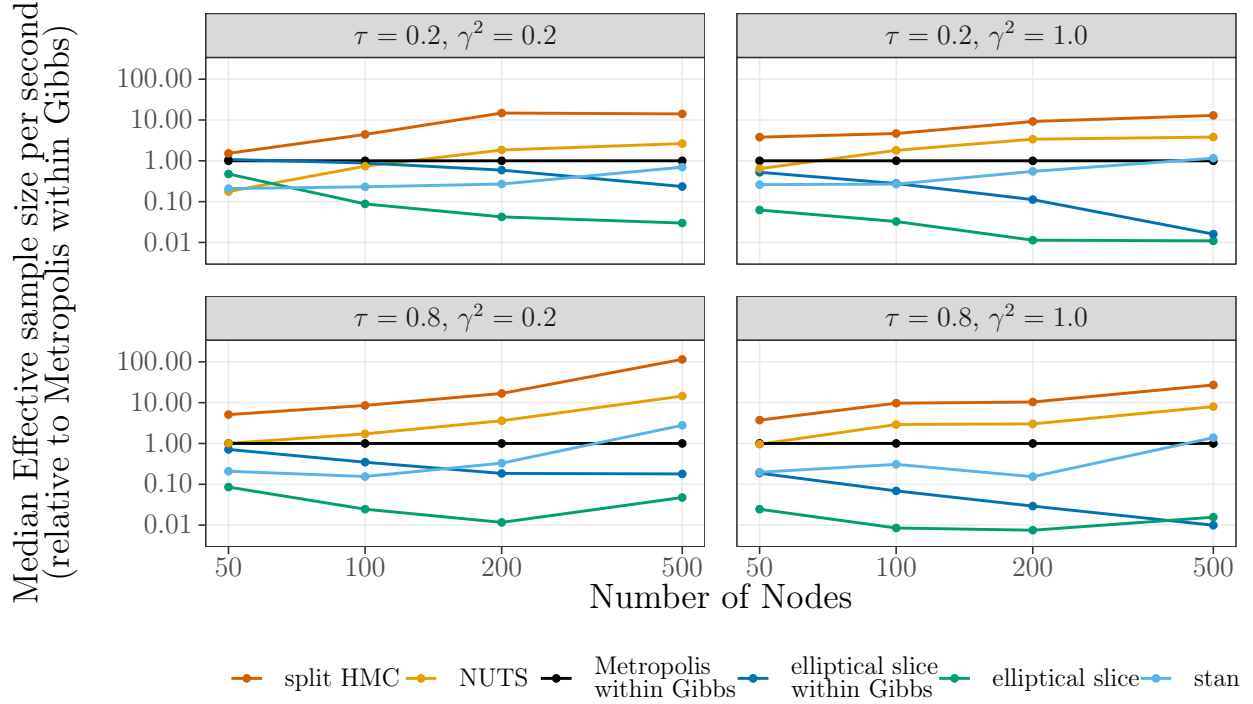


Figure 1: A depiction of the relationship between the number of nodes in the synthetically generated networks ($\tau = 0.2, 0.8, \gamma^2 = 0.2, 1.0$) for Empirical Study 1 and the relative efficiency (compared to Metropolis within Gibbs) of the five posterior computation algorithms. For each algorithm, relative efficiency (y axis) is quantified as the median across 500 dyads in the synthetic network of the relative Markov chain efficiency compared to Metropolis within Gibbs. For readability, the results from the analogous FlyMC algorithms are presented separately as Figure 2, using the same colors (but dashed instead of solid lines).

demonstrating that the extra computational cost of these strategies adaptively updating L may be unwarranted for LPMs.

All methods based on elliptical slice sampling perform poorly, demonstrating that HMC is a better method for exploiting the near-Gaussianity of the posterior than elliptical slice sampling. Indeed, the elliptical slice sampling algorithms performed worse than Metropolis within Gibbs. The poor performance of the elliptical slice within Gibbs algorithms was due to its runtime—the conditional means and variances of each latent position at each iteration

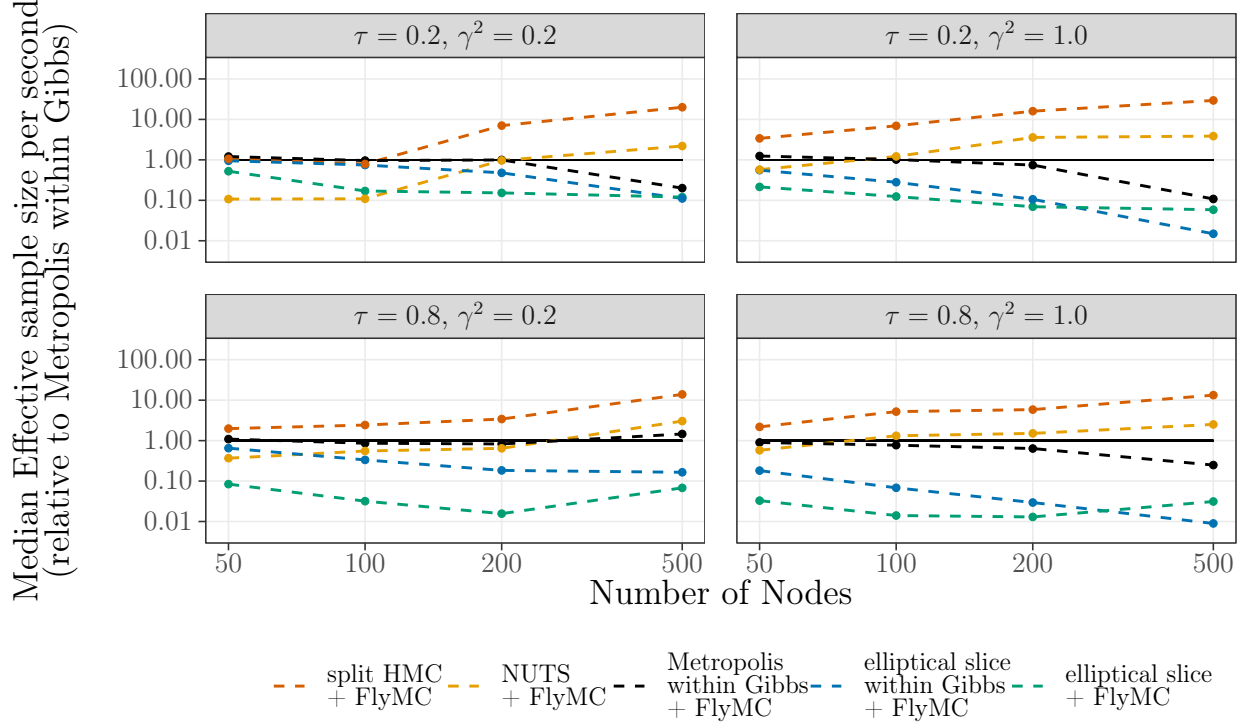


Figure 2: A depiction of the relationship between the number of nodes in the synthetically generated networks ($\tau = 0.2, 0.8, \gamma^2 = 0.2, 1.0$) for Empirical Study 1 and the relative efficiency (compared to Metropolis within Gibbs) of the five FlyMC posterior computation algorithms. This figure is a companion to Figure 1, presenting the same metric. The solid black baseline is included for easy comparison to Metropolis within Gibbs.

are very expensive to compute. The joint update elliptical slice algorithms performed poorly for the opposite reason. They had much faster runtimes, but the corresponding chains mixed very slowly because the draws exhibited very high autocorrelation.

It is also worth noting that the dominance of the Split HMC methods are more pronounced for larger networks—Split HMC and Split HMC + FlyMC are on the order of 50 to 100 times more efficient than Metropolis within Gibbs for 500 node networks. For the denser $\tau = 0.8$ networks, standard Split HMC performs remarkably well, showing a distinct upward trend, indicating that its dominance over Metropolis within Gibbs would be even more pronounced for larger networks. For the sparser $\tau = 0.2$ networks, Split

HMC + FlyMC demonstrates a similar upward trend. The tuned values of ϵ and δ shown in Figure 6 in Section 6.3 of the Appendix demonstrate that split HMC is more robust to large network sizes: while the tuned step sizes for the Metropolis within Gibbs decay as the number of nodes increases, the tuned values of ϵ for split HMC remain more stable.

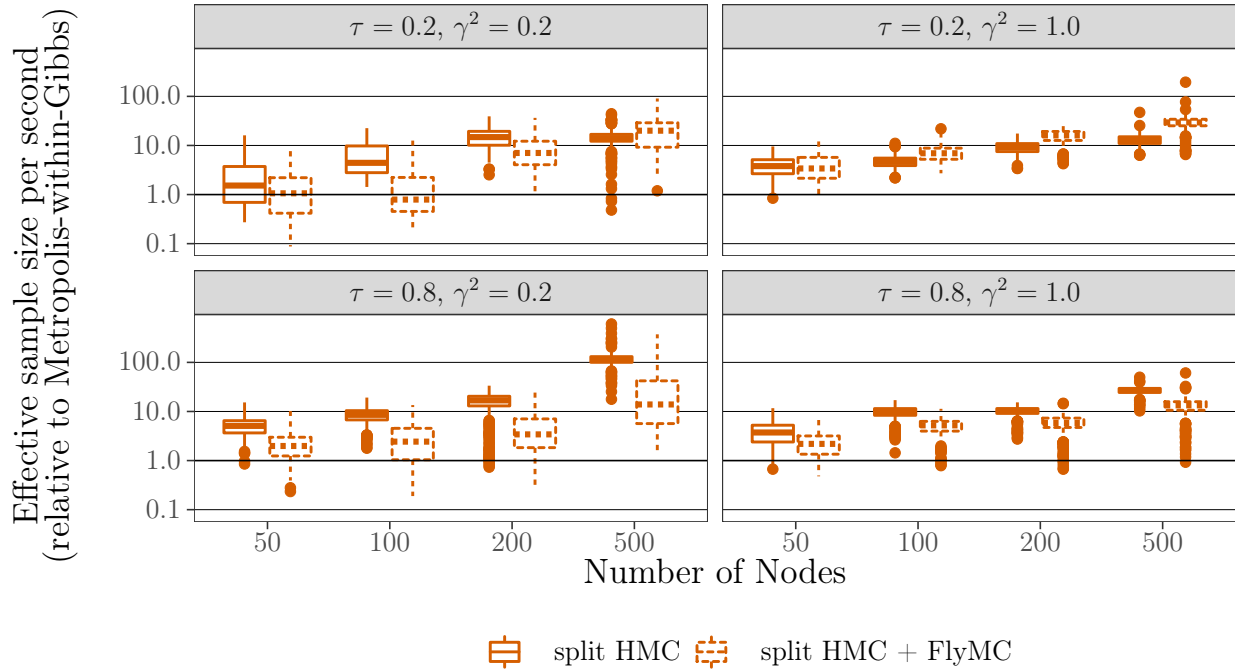


Figure 3: Boxplots summarizing the distribution of relative efficiency of Split HMC + FlyMC and standard Split HMC relative to Metropolis within Gibbs across 500 dyads in each network.

To facilitate comparison between the FlyMC and standard implementations of split HMC, we have also included Figure 3. Instead of just reporting the median, it summarizes the entire distribution of (44) across the 500 sampled dyads. From the side-by-side boxplots, we can see that standard split HMC clearly outperforms split HMC + FlyMC for the $\tau = 0.8$ networks of all sizes. For the $\tau = 0.2$ networks, the comparison is less clear cut. For the very sparse network $\tau = 0.2, \gamma^2 = 0.2$, standard split HMC outperforms the FlyMC version for the smaller networks, but FlyMC edges it out for the 500 node network. It is worth noting that in this very sparse regime for smaller networks, the extreme lack of edges can lead to

ambiguity in whether the extreme sparsity is driven by small τ , small γ^2 , or both. The joint posteriors of τ, γ^2 for different synthetic networks shown in Figure 7 (Section 6.3 of the Appendix) demonstrates this phenomenon—there is a remarkable amount of uncertainty in the posterior of τ for the smaller sparse networks.

We have noticed that the FlyMC updates of τ and θ tend to mix slowly in these uncertain situations, thus leading to slow exploration of the joint distribution of (τ, γ^2) . Unencumbered by slow-mixing θ variables, standard FlyMC tends to perform better in these under-identified settings, suggesting that FlyMC should only be used when the τ variable is better identified. This seems to be the case in the $\tau = 0.2, \gamma^2 = 1.0$ networks, where the FlyMC clearly outperforms the standard version.

The full distribution of the relative efficiencies highlights another observation—although the split HMC algorithms tend to outperform Metropolis within Gibbs for the vast majority of dyads, there is often a small minority of dyads for which Metropolis within Gibbs performs better (seen as the lower tails of the boxplots sometimes extending below 1). A thorough investigation into these dyads revealed no apparent pattern for which dyads tend to perform relatively poorly in a given network, suggesting that the primary explanation is simply the high-dimensionality of the posterior—with so many dimensions along which to mix, there will often be a small minority that mix more slowly. Regardless, the under-performance is not drastic for the large networks in which we are interested—split HMC still performs at the same order of magnitude as Metropolis within Gibbs.

From this empirical study, we have demonstrated that split HMC and split HMC + FlyMC tend to outperform competitors in the literature on synthetically generated data. For denser networks, or networks for which τ and γ^2 are poorly identified (i.e. smaller sparse networks), standard split HMC tends to be the better choice. For larger sparse networks, split HMC + FlyMC seems to be the top performer. In all cases, using these strategies will perform far better than simple Metropolis within Gibbs.

However, there is no guarantee that good performance on these synthetically generated networks (i.e. perfectly specified models) will necessarily translate to good performance on the approximately specified models that occur in real data applications. For this reason, we

now turn to Study 2, where we use our algorithms to fit LPMs to real data with categorical covariates and structured priors.

4.3 Study 2: Network of Information-sharing in a School District

To demonstrate the efficacy of our split Hamiltonian Monte Carlo strategies applied to real data, we now showcase several applications of LPMs to information-sharing networks of teachers and staff in a school district. These applications involve several model/network configurations commonly encountered in practice: networks with categorical covariates that encode known group memberships of the nodes, longitudinally-observed networks with models enforcing serial dependence of the latent positions, and combinations of the two. The data we use in these applications were collected as part of the Distributed Leadership Studies at Northwestern University, a comprehensive program of research involving several longitudinal studies of workplace and social interactions among school staff and school systems. For more details about this particular dataset, see Spillane and Hopkins [2013]; Spillane et al. [2018].

The networks we use pertain to Auburn Park, a pseudonym for a mid-sized suburban school district in the Midwestern United States. In five separate years, elementary school teachers and staff within this district were surveyed about who in the district they went to for advice, as well as the school in which they worked and other relevant covariates (e.g. what subjects they taught). Over these years, 661 distinct individuals responded to this advice-seeking survey in at least one year. 129 of them were present for all five surveys (some left or entered the district during the survey years).

For the purposes of this empirical study, we have compiled the survey responses into a series of five undirected *information-sharing* networks—one for each year of data. These undirected information-sharing relationships were obtained by symmetrizing the information in the advice-seeking survey. That is, for each network, an edge is present between two individuals if either of them reported going to the other for advice in that year. In addition to the edge information, we have are covariates indicating which individuals worked in the same school in each year (covariate a), and whether or not they had shared information in

the previous survey year (covariate b).

From this sequence of networks, we have extracted four different subnetworks:

- *One school, one year*: the information-sharing network of 32 teachers and staff working within the same school (school ID 4) in the first survey year.
- *All schools, one year*: the information-sharing network of 326 teachers and staff across all fourteen schools in the district in the first survey year.
- *One school, all years*: a series of five information-sharing networks of fourteen teacher and staff working within the same school (school ID 4). Each network corresponds to a different survey year.
- *All schools, all years*: a series of five information-sharing networks of 129 teachers and staff working across all fourteen schools in the district. Each network corresponds to a different survey year.

Using these subnetworks, we fit six different models (one model for each of the *one school, one year* and *one school, all years* networks, and two models for each of the *all schools, one year* and *all schools, all years* networks). These models represent six separate settings with which to assess the performance of standard split HMC and split HMC with FlyMC. The specifics of how these four datasets were constructed, as well as the details of the six models we fit to them, are provided below (for quick reference, a summary is available in Table 1). For each model fit, the efficiency of Split HMC and Split HMC with FlyMC are reported in Figure 4, relative to the baseline Metropolis within Gibbs.

The *one school, one year* network corresponds to all information shared within a specific school in the district (shown as school ID 4 in Figure 5) in survey year one. We chose this particular school due because it contains a large number of teachers and staff who were interviewed in all five years. To this network, we fit one model—a Gaussian LPM with no covariates, an independent two-dimensional isotropic Gaussian priors for each z_i , a uniform prior on τ , and an inverse gamma (IG(1,1)) prior on γ^2 .

The *all schools, one year* network represents all information shared across all schools in the district (both between and within-schools) in survey year one. To this network, we

Model	Number of Schools	Number of Years	Number of Nodes	Number of Edges	Covariate
one year one school	1	1	32	150	No covariate
one year, all schools	14	1	326	1363	No covariate
one year, all schools covariate a	14	1	326	1363	Indicator for whether or not individuals work at the same school
all years, one school covariate b	1	5	14 per year	79	Indicator for whether or not individuals shared info in the previous year
all years, all schools covariate b	14	5	129 per year	1038	Indicator for whether or not individuals shared info in the previous year
all years, all schools a, b	14	5	129 per year	1038	Indicator for whether or not individuals work at the same school <i>and</i> Indicator for whether or not individuals shared info in the previous year

Table 1: A summary of the model and data configurations for Empirical Study 2

fit two separate LPMs: one without covariates, and another in which the binary covariate a is used to indicate whether or not the two individuals were working in the same school that year. For both model configurations, we used independent two-dimensional isotropic Gaussian priors for each z_i , a bivariate uniform prior on τ , and an inverse gamma (IG(1,1)) prior on γ^2 .

For the *one school, all years* network, we considered the same school (school ID 4) as in the *one school, one year* network. However, we included only those 14 teachers and staff that were surveyed in that school in all five survey years—any individuals that missed at least one survey year or changed schools during the study were excluded. As a result, this data consists of a series of five networks on the same 14 nodes across the five survey years. We fit one model to these five years data—a single longitudinal latent position model [Kim et al., 2018]. Doing so is straightforward within our LPM framework; we pooled the five distinct fourteen node networks into a single 70 node network, then treated any of the impossible “across year” dyads (e.g. a year 1 node cannot share information with a year 3 node) as unobserved, omitting them from the likelihood. We model the temporal dependence in the network in two ways. First, we place an autoregressive prior on each nodes’ sequence of two-dimensional latent positions—a Gaussian prior where subsequent years are autocorrelated at a 0.95 level. Second, we use the binary covariate b to allow the model to account for “persistent edges”. That is, b indicates whether or not the edge being considered was present in the previous year. As before, we place independent uniform priors on each value of $\tau \in [0, 1]^2$, and an inverse gamma (IG(1,1)) prior on γ^2 .

Finally, the *all schools, all years* is sequence of five networks similar to the *one school, all years* network but with all schools in the district considered. Like for the *one school, all years* network, this network includes only those that were surveyed in all five years. However, we do keep those who changed schools within the district (updating their covariates year-to-year). For this data, we fit two separate models for *all schools, all years*. They are analogous to the two models considered for *all schools, one year* but they also incorporate longitudinal dependence as in the *one school, all years* model. That is, both *all schools, all years* models involve a two-dimensional Gaussian prior to enforce 0.95 serial correlation

among an individual's latent position in adjacent survey years. The two models differ in how their covariates are structured. One model, analogous to the “no covariate” model for *all schools, one year*, uses just the binary covariate b to indicate whether the edge was present in the previous year (as in the *one school, all years* model). The second model, analogous to the covariate model for *all schools, one year*, incorporates the covariate information from both a and b : x_{ij} takes on four separate values. The values depend on whether or not the teachers/staff work in the same school (a) and whether or not the edge was present in the previous survey year (b).

Note that we chose and structured the datasets and models above to ensure simplicity; they allow us to consider different LPM set-ups in the study without having to account for irregularly missing data or any potential artifacts thereof.

For all six models, we employed the same preliminary run tuning strategy as in Study 1 (Section 4.2) to choose ϵ for the split HMC algorithms (with $T \approx 2$), as well as the random-walk step size for each parameter in the Metropolis within Gibbs and the update of τ in standard split HMC. Each Metropolis within Gibbs chain was run for 20000 iterations, and each standard HMC and HMC + FlyMC chain was run for 10000 iterations. For each algorithm and model, the distribution of relative speed-up (as measured by (44)) is summarized using a boxplot for 500 randomly selected dyads in Figure 4 (all 496 unique dyads for the one year one school network are shown).

In each of the six settings, both the standard and FlyMC versions of split HMC vastly outperform Metropolis within Gibbs, even more so than in Study 1. The speed-up is most pronounced in the all years, all schools with covariates a and b setting, where both algorithms are almost 1000 times more efficient than Metropolis within Gibbs. For the most part, the two HMC algorithms (with and without FlyMC) perform comparably across the different model/data settings. The most noticeable difference occurs in the two models fit to the one year, all schools network. Without the covariate a , standard split HMC performs better. When a is included, the FlyMC version is the better performer. This disparity between the two models provides a good case study for when FlyMC is most useful, so we will now dig deeper into how the inclusion/exclusion of the covariate affects

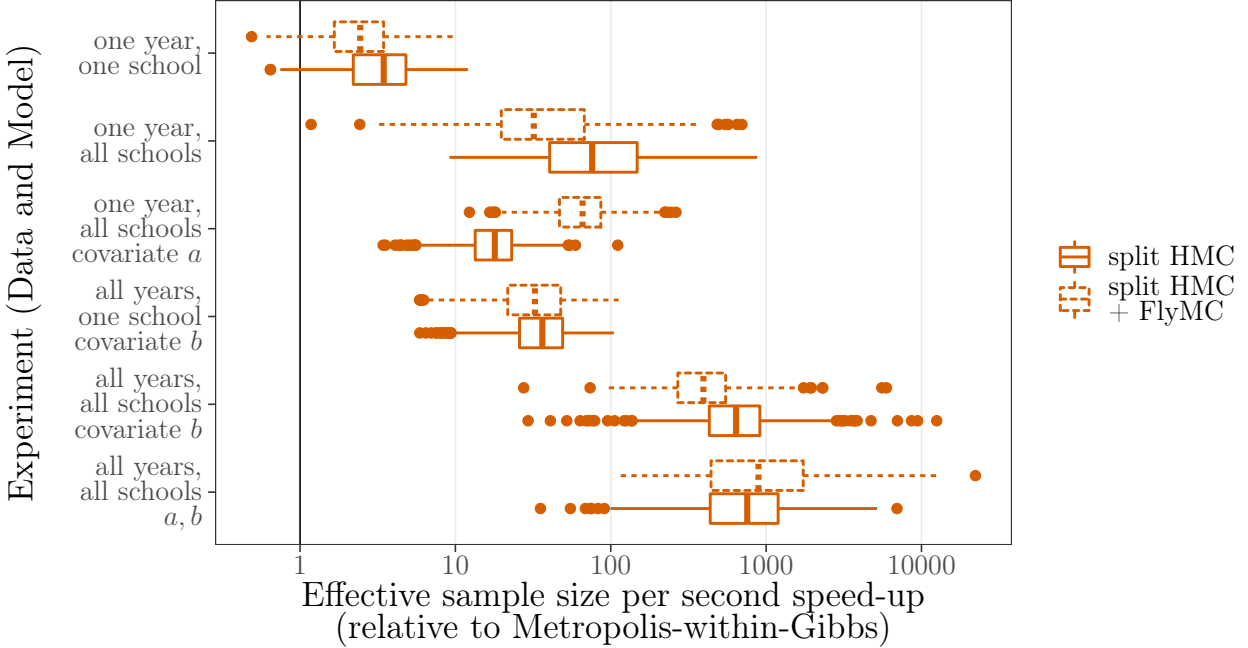


Figure 4: Boxplots depicting the relative efficiency (in terms of effective sample size per second) of split Hamiltonian Monte Carlo (both with and without FlyMC) compared to Metropolis within Gibbs. The six different data/model configuration described above are considered. For each configuration, the relative speed-up in effective sample size per second is provided for computing the posterior log probability of a random subset of 500 dyads in the network. Note that the x-axis is provided on the log scale.

the model fits and Monte Carlo algorithms.

Figure 5 summarizes the fits of the two separate models on the one year, all schools network. For both models, the nodes are arranged according to point estimates of their latent positions. These point estimates were obtained by computing the expectation of the matrix of squared distances between the latent positions, then using multi-dimensional scaling to extract the optimal two-dimensional embedding based on these distances. Contours of the posterior distribution for three nodes at different schools are included to demonstrate the uncertainty in the corresponding posteriors. These contours were obtained by applying a Procrustes transformation to all of the posterior samples to best align them with the point

estimates of the latent positions.

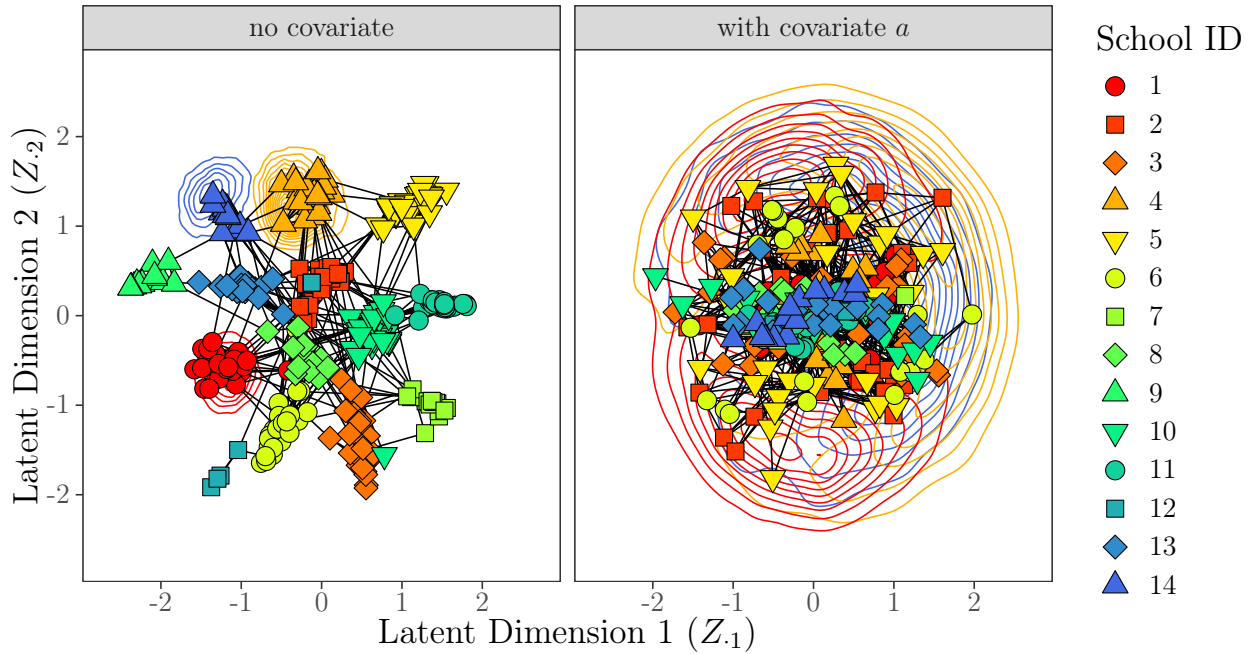


Figure 5: The left panel depicts point estimates of the nodes' latent positions in the one year, all schools model. The right panel depicts point estimates of the nodes' latent positions in the one year, all schools, covariate a model. Both sets of point estimates are obtained via 2-dimensional multi-dimensional scaling on the corresponding posterior expectation of the matrix of squared latent distances. In both plots, each node's shape/color combination is assigned according to the individual's school. Uncertainty contours of the latent positions are depicted for three individuals at different schools (one from school 1, one from school 4, one from school 14—the contours are colored according to school). Finally, the information-sharing relationships are included as edges.

Figure 5 demonstrates that information-sharing tends to be mostly concentrated within schools. The school information is unavailable in the no covariate model, but the LPM still manages to capture the strength of this effect using the latent positions. Their estimated values effectively act as a proxy for the held-out covariate information, clustering the individuals in space according to the schools at which they work. The posterior expectation

of γ^2 for this model is thus quite small (a posterior expected value of approximately 0.15) ensuring the link probability function decays rapidly to capture the rarity of edges between clusters. With most nodes' latent positions tending to be close to others within the same school, the value of τ in this model effectively captures the rate of within-school ties—its posterior expected value in the model is approximately 0.43. The few between-school ties that are present in the network determine the relative positioning of the different school clusters in the posterior fit.

Explicitly including the school covariate a in the model leads to a much different fit of the latent positions. Because the estimated value of τ directly captures the large disparity between the within-school edge density and between-school edge density (τ has a posterior mean of 0.86 for within-school ties versus 0.01 for between-school ties), the latent positions are free to capture any residual structure in the network. The corresponding posterior shown in Figure 5 is diffuse and unstructured—the uncertainty contours for the three nodes covers most of the nodes' estimated latent positions. This suggests that the majority of the network's structure is captured by the covariate. Accordingly, the posterior expected value of γ^2 in this setting is approximately 1.19—much larger than the no covariate setting—showing that the edge probabilities decay more gradually with latent distance.

The superior performance of the FlyMC algorithm in the covariate a setting is due to its ability exploit the sparsity (modeled by τ) between schools. The corresponding θ variables drastically downsample the number of dyads involved in each likelihood and gradient calculation, speeding up computation. This illustrates that FlyMC is especially useful when applied to dyads for which the value of $\tau_{x_{ij}}$ is expected to be small.

Shifting focus to the *all years, all schools* models, an inspection of their fits reveals that the models with and without a differ in a similar way to the one year models. For the model without covariate a , the posterior means of the τ variables are 0.27 (when the previous year is a non-edge) and 0.96 (when the previous year is an edge). The posterior mean of γ^2 is 0.18, reflecting the same tight separation of the latent positions into within-school clusters. For model with covariate a , the posterior means of the τ variables are 0.01 (for a between-school dyads when the previous year is a non-edge), 0.74 (for a within-school dyad when

the previous year was a non-edge), 0.32 (for a between-school edge when the previous year was an edge), and 0.86 (for a within-school edge when the previous year was an edge). Again, the τ variable captures most of the structure in the network. The posterior mean of γ^2 is 1.09. For both of these longitudinal models, the particularly strong performance of the split HMC algorithms compared to Metropolis within Gibbs can be attributed to two factors: the size of the network, and the extra structure imposed by the temporal autocorrelation in latent positions. The joint gradient-informed update of all nodes in split HMC is particularly well-suited to account for the autocorrelation in the prior, where the uninformed random walk update of Metropolis within Gibbs is not.

Surprisingly, despite the small value of the between-schools τ for the model with covariate a , we do not see much of a disparity between the performance of the standard and FlyMC implementations of split HMC when fitting the all years, all schools, covariates a, b model. This is due partially to the slower mixing of the τ variables in the FlyMC implementations than in the standard implementation—although they facilitate a closed-form Gibbs update, the auxiliary θ variables can also lead to extra autocorrelation in the chains for τ as they slowly evolve. Another contributor to the smaller disparity is a larger gap between tuned values of ϵ . Our approach for tuning ϵ and L yielded $\epsilon = 0.31$, $L = 7$ for the standard implementation, and $\epsilon = 0.14$ and $L = 15$ for the FlyMC implementation. In the corresponding one year models, the gap was not as large— $\epsilon = 0.22$, $L = 10$ for the standard implementation compared to $\epsilon = 0.14$ and $L = 15$ for the FlyMC implementation.

5 Concluding Remarks

In this article, we proposed a new algorithm based on a split HMC for inferring the latent positions in Gaussian LPMs, as well as strategies for updating the parameters of the link function (4). Moreover, we described an auxiliary FlyMC algorithm for subsampling the non-edge dyads while keeping the Monte Carlo algorithm exact. We conducted two empirical studies to investigate the performance of the split HMC and split HMC + FlyMC approaches: one on synthetic data (Section 4.2) and one on real data concerning information-sharing among teachers and staff (Section 4.3).

Our synthetic data study demonstrated that when split HMC and split HMC + FlyMC are tuned to have an acceptance rate of around 0.8-0.85 (for $T \approx 2$), these algorithms vastly outperform similarly well-tuned competitors in the literature, especially for large networks. The competitors we considered included standard algorithms such as Metropolis within Gibbs and elliptical slice sampling, as well as more sophisticated HMC algorithms such as the NUTS and Stan that adaptively set T . Across the board, our implementations of split HMC and split HMC + FlyMC outperformed all competitors, even the more sophisticated HMC algorithms. Of the two new algorithms proposed in this article, standard split HMC seemed to be the better performer for denser networks, as well as smaller sparse networks for which the link function parameters were poorly identified. Split HMC + FlyMC performs best on large, sparse networks that contain sufficient information to identify the link function parameters. Given these results, we would expect split HMC + FlyMC to perform especially well in settings for which τ is very small, such as the sparse graphon version of GLPMs [Borgs et al., 2014, Spencer and Shalizi, 2019].

At first, we were surprised by the extent to which the HMC integration time T at approximately 2 outperformed the adaptive strategies for setting T used in NUTS and Stan. Adaptive strategies have been shown to perform outperform fixed integration strategies across a variety of models and perform at least comparably for others [Hoffman and Gelman, 2014, Betancourt, 2016]. However, the relatively poor performance of these algorithms on LPMs is less surprising when one considers the criteria used by Stan and NUTS to choose T . Both algorithms are configured to optimize the mixing of the latent positions. However, as we discussed in Section 4.1, the latent positions themselves are under-identified in the posterior—the edge probabilities or latent distances are more appropriate targets. This insight suggests a potential avenue of future research—perhaps an adaptation of the NUTS criterion that optimizes the mixing of user-specified functions of the parameters would be a worthwhile extension.

The real data studies involving covariates in Section 4.3 demonstrated FlyMC also performs well when τ is allowed to vary by a categorical covariate, taking on small values for just some categories of the covariate. Another potential avenue of future research would

be to consider a hybrid of standard split HMC and split HMC + FlyMC. FlyMC would be applied to a subset of the dyads, such as those possessing covariate categories for which τ is expected to be small. This would for FlyMC to be exploited where it is most effective, while limiting any potential mixing problems due to the introduction of additional auxiliary variables.

In Study 2, we also considered the application of our algorithm to fit Gaussian LPMs for longitudinal networks. Of the variety of different ways to configure longitudinal LPMs [Kim et al., 2018], we used a simple model structure that used a structured Gaussian prior to promote serial dependence of the nodes' latent positions across time points, as well as covariates to promote persistent edges across time points. For these models, our split HMC algorithm performed particularly well because gradient-informed proposals naturally accommodate the extra structure in the prior. Therefore, we anticipate that our insights could also be applied to achieve substantial computational gains in other more structured priors for LPMs, such as latent cluster model [Krivitsky et al., 2009] or the multi-resolution network model Fosdick et al. [2018]. Recently, Turnbull [2020] explored the use of sequential Monte Carlo [Doucet and Johansen, 2009] for Bayesian inference of longitudinal latent position models. They found that the scaling of the algorithm was poor for large networks due to the computational complexity of evaluating the likelihood. These findings suggest that a combination of their approach with the algorithms we present here could be fruitful.

Finally, it is worth briefly commenting on our motivation for focusing on Gaussian link function instead of the traditional logistic link function. When proposing the GLPM, Rastelli et al. [2016] argued that the Gaussian LPM yields results that are analogous and comparable to those of the logistic LPM, whilst providing interpretable link function parameters and making it easier to derive theoretical results. Since then, Spencer and Shalizi [2019] proved consistent estimation results for the Gaussian link function—analogous results under the logistic link function remain an open problem. In this article, we have demonstrated additional benefits of the Gaussian link function over the logistic link function. The closed-form Gaussian decomposition underlying our split HMC algorithm is not possible with a logistic link, and the FlyMC strategy cannot be applied because it relies on

a factorization of the sparsity parameter τ from the link function. Moreover, the likelihood of the logistic link LPM is not differentiable when two nodes have the same position, which complicates the application of HMC at all. For all of these reasons, we propose that the Gaussian LPM would be a more suitable “default” choice of the link function—the logistic link should only be used when its particular functional form is justified by the application.

Acknowledgements

We would like to acknowledge helpful suggestions and feedback from Robert Kass, Jared Murray, Cosma Shalizi, participants of the Networkshop research group at Carnegie Mellon University, the audience at the Statistical Inference in Network Models satellite symposium of NetSci 2019, seminar attendees at Dalhousie University, and those who visited our poster at the OBayes17 conference.

We would like to thank Alex Reinhart, Carl Skipper, posters on The Stan Forum, and Roberto Gomez for their help and guidance regarding how to design and run the empirical studies in a supercomputing environment. This work used the Extreme Science and Engineering Discovery Environment (XSEDE), which is supported by National Science Foundation grant number ACI-1548562. Specifically, it used the Bridges system, which is supported by NSF award number ACI-1445606, at the Pittsburgh Supercomputing Center (PSC).

Finally, we would like acknowledge Jim Spillane and the Distributed Leadership Studies (<http://www.distributedleadership.org>) at Northwestern University, including the NebraskaMATH study, for the use of their data in this work. We greatly appreciate the help provided by Jim and his colleagues.

References

Edoardo M Airoldi, David M Blei, Stephen E Fienberg, and Eric P Xing. Mixed membership stochastic blockmodels. *Journal of machine learning research*, 9(Sep):1981–2014, 2008.

Emanuele Aliverti and Daniele Durante. Spatial modeling of brain connectivity data via latent distance models with nodes clustering. *Statistical Analysis and Data Mining: The ASA Data Science Journal*, 12(3):185–196, 2019.

Ben Bales, Arya Pourzanjani, Aki Vehtari, and Linda Petzold. Selecting the metric in hamiltonian monte carlo. *arXiv preprint arXiv:1905.11916*, 2019.

Michael Betancourt. Identifying the optimal integration time in hamiltonian monte carlo. *arXiv preprint arXiv:1601.00225*, 2016.

Michael Betancourt. A conceptual introduction to hamiltonian monte carlo. *arXiv preprint arXiv:1701.02434*, 2017.

Benjamin Bloem-Reddy and John Cunningham. Slice sampling on hamiltonian trajectories. In *International Conference on Machine Learning*, pages 3050–3058, 2016.

Christian Borgs, Jennifer Chayes, Henry Cohn, and Yufei Zhao. An l^p theory of sparse graph convergence i: Limits, sparse random graph models, and power law distributions. *Transactions of the American Mathematical Society*, 01 2014. doi: 10.1090/tran/7543.

Bob Carpenter, Andrew Gelman, Matthew D Hoffman, Daniel Lee, Ben Goodrich, Michael Betancourt, Marcus Brubaker, Jiqiang Guo, Peter Li, and Allen Riddell. Stan: A probabilistic programming language. *Journal of statistical software*, 76(1), 2017.

Peter J Carrington, John Scott, and Stanley Wasserman. *Models and methods in social network analysis*, volume 28. Cambridge university press, 2005.

Wei-Lun Chao, Justin Solomon, Dominik Michels, and Fei Sha. Exponential integration for hamiltonian monte carlo. In *International Conference on Machine Learning*, pages 1142–1151, 2015.

Li Chen, Joshua T Vogelstein, Vince Lyzinski, and Carey E Priebe. A joint graph inference case study: the *c. elegans* chemical and electrical connectomes. In *Worm*, volume 5, page e1142041. Taylor & Francis, 2016.

Grace S Chiu and Anton H Westveld. A unifying approach for food webs, phylogeny, social networks, and statistics. *Proceedings of the National Academy of Sciences*, 108(38):15881–15886, 2011.

Aaron Clauset, Cristopher Moore, and Mark EJ Newman. Hierarchical structure and the prediction of missing links in networks. *Nature*, 453(7191):98, 2008.

Harry Crane. *Probabilistic foundations of statistical network analysis*. Chapman and Hall/CRC, 2018.

Beau Dabbs, Samrachana Adhikari, and Tracy Sweet. Conditionally independent dyads (cid) network models: a latent variable approach to statistical social network analysis. *Social Networks*, Revision Under Review, 2020.

Perry de Valpine. How we make mcmc comparisons. https://nature.berkeley.edu/~pdevalpine/MCMC_comparisons/nimble_MCMC_comparisons.html, 2018. Accessed: 2020-04-24.

Arnaud Doucet and Adam M Johansen. A tutorial on particle filtering and smoothing: Fifteen years later. *Handbook of nonlinear filtering*, 12(656-704):3, 2009.

Simon Duane, Anthony D Kennedy, Brian J Pendleton, and Duncan Roweth. Hybrid monte carlo. *Physics letters B*, 195(2):216–222, 1987.

Paul Erdős and Alfréd Rényi. On the evolution of random graphs. *Publ. Math. Inst. Hung. Acad. Sci.*, 5(1):17–60, 1960.

Bailey K Fosdick, Tyler H McCormick, Thomas Brendan Murphy, Tin Lok James Ng, and Ted Westling. Multiresolution network models. *Journal of Computational and Graphical Statistics*, pages 1–12, 2018.

Dani Gamerman and Hedibert F Lopes. *Markov chain Monte Carlo: stochastic simulation for Bayesian inference*. CRC Press, 2006.

Andrew Gelman, John B Carlin, Hal S Stern, David B Dunson, Aki Vehtari, and Donald B Rubin. *Bayesian data analysis*. CRC press, 2013.

Mark Girolami and Ben Calderhead. Riemann manifold langevin and hamiltonian monte carlo methods. *Journal of the Royal Statistical Society: Series B (Statistical Methodology)*, 73(2):123–214, 2011.

Anna Goldenberg, Alice X Zheng, Stephen E Fienberg, Edoardo M Airoldi, et al. A survey of statistical network models. *Foundations and Trends® in Machine Learning*, 2(2):129–233, 2010.

P Richard Hahn, Jingyu He, and Hedibert F Lopes. Efficient sampling for gaussian linear regression with arbitrary priors. *Journal of Computational and Graphical Statistics*, 28(1):142–154, 2019.

Mark S Handcock, Adrian E Raftery, and Jeremy M Tantrum. Model-based clustering for social networks. *Journal of the Royal Statistical Society: Series A (Statistics in Society)*, 170(2):301–354, 2007.

Michael Hecker, Sandro Lambeck, Susanne Toepfer, Eugene Van Someren, and Reinhard Guthke. Gene regulatory network inference: data integration in dynamic models—a review. *Biosystems*, 96(1):86–103, 2009.

Peter D Hoff, Adrian E Raftery, and Mark S Handcock. Latent space approaches to social network analysis. *J. Am. Stat. Association*, 97(460):1090–1098, 2002.

Matthew D Hoffman and Andrew Gelman. The no-u-turn sampler: adaptively setting path lengths in hamiltonian monte carlo. *Journal of Machine Learning Research*, 15(1):1593–1623, 2014.

Pengsheng Ji and Jiashun Jin. Coauthorship and citation networks for statisticians. *The Annals of Applied Statistics*, 10(4):1779–1812, 2016.

Robert E Kass, Bradley P Carlin, Andrew Gelman, and Radford M Neal. Markov chain monte carlo in practice: a roundtable discussion. *The American Statistician*, 52(2):93–100, 1998.

Bomin Kim, Kevin H Lee, Lingzhou Xue, and Xiaoyue Niu. A review of dynamic network models with latent variables. *Statistics surveys*, 12:105, 2018.

Pavel N Krivitsky and Mark S Handcock. Fitting position latent cluster models for social networks with latentnet. *Journal of Statistical Software*, 24, 2008.

Pavel N Krivitsky, Mark S Handcock, Adrian E Raftery, and Peter D Hoff. Representing degree distributions, clustering, and homophily in social networks with latent cluster random effects models. *Social networks*, 31(3):204–213, 2009.

Benedict Leimkuhler and Sebastian Reich. *Simulating hamiltonian dynamics*, volume 14. Cambridge university press, 2004.

Scott Linderman, Ryan P Adams, and Jonathan W Pillow. Bayesian latent structure discovery from multi-neuron recordings. In *Advances in neural information processing systems*, pages 2002–2010, 2016.

Samuel Livingstone, Michael Betancourt, Simon Byrne, Mark Girolami, et al. On the geometric ergodicity of hamiltonian monte carlo. *Bernoulli*, 25(4A):3109–3138, 2019.

Dougal Maclaurin and Ryan Prescott Adams. Firefly Monte Carlo: Exact MCMC with subsets of data. In *International Joint Conference on Artificial Intelligence*, 2015.

Oren Mangoubi and Aaron Smith. Rapid mixing of hamiltonian monte carlo on strongly log-concave distributions. *arXiv preprint arXiv:1708.07114*, 2017.

Oren Mangoubi and Aaron Smith. Mixing of hamiltonian monte carlo on strongly log-concave distributions 2: Numerical integrators. In *The 22nd International Conference on Artificial Intelligence and Statistics*, pages 586–595, 2019.

Janne Mannseth, Tore Selland Kleppe, and Hans J Skaug. On the application of higher order symplectic integrators in hamiltonian monte carlo. *arXiv preprint arXiv:1608.07048*, 2016.

Iain Murray, Ryan Adams, and David MacKay. Elliptical slice sampling. In *Proceedings of the Thirteenth International Conference on Artificial Intelligence and Statistics*, pages 541–548, 2010.

Radford M Neal. *MCMC using Hamiltonian dynamics*, chapter 5. 2011.

Mark EJ Newman. Spread of epidemic disease on networks. *Physical review E*, 66(1):016128, 2002.

Nicholas A Nystrom, Michael J Levine, Ralph Z Roskies, and J Ray Scott. Bridges: a uniquely flexible hpc resource for new communities and data analytics. In *Proceedings of the 2015 XSEDE Conference: Scientific Advancements Enabled by Enhanced Cyberinfrastructure*, pages 1–8, 2015.

Ari Pakman and Liam Paninski. Exact hamiltonian monte carlo for truncated multivariate gaussians. *Journal of Computational and Graphical Statistics*, 23(2):518–542, 2014.

Omiros Papaspiliopoulos, Gareth O Roberts, and Martin Sköld. A general framework for the parametrization of hierarchical models. *Statistical Science*, pages 59–73, 2007.

Martyn Plummer, Nicky Best, Kate Cowles, and Karen Vines. Coda: convergence diagnosis and output analysis for mcmc. *R news*, 6(1):7–11, 2006.

Adrian E Raftery, Xiaoyue Niu, Peter D Hoff, and Ka Yee Yeung. Fast inference for the latent space network model using a case-control approximate likelihood. *Journal of Computational and Graphical Statistics*, 21(4):901–919, 2012.

Riccardo Rastelli, Nial Friel, and Adrian E Raftery. Properties of latent variable network models. *Network Science*, 4(4):407–432, 2016.

Riccardo Rastelli, Florian Maire, and Nial Friel. Computationally efficient inference for latent position network models. *arXiv preprint arXiv:1804.02274*, 2018.

Brian D Ripley. *Stochastic simulation*, volume 316. John Wiley & Sons, 2009.

Gareth Roberts, Jeffrey Rosenthal, et al. Geometric ergodicity and hybrid markov chains. *Electronic Communications in Probability*, 2:13–25, 1997.

Gareth O Roberts, Jeffrey S Rosenthal, et al. Optimal scaling for various metropolis-hastings algorithms. *Statistical science*, 16(4):351–367, 2001.

Jeffrey S. Rosenthal. Simple confidence intervals for mcmc without clts. *Electron. J. Statist.*, 11(1):211–214, 2017. doi: 10.1214/17-EJS1224. URL <https://doi.org/10.1214/17-EJS1224>.

Michael Salter-Townshend and Tyler H McCormick. Latent space models for multiview network data. *The annals of applied statistics*, 11(3):1217, 2017.

Michael Salter-Townshend and Thomas Brendan Murphy. Variational bayesian inference for the latent position cluster model for network data. *Computational Statistics & Data Analysis*, 57(1):661–671, 2013.

Babak Shahbaba, Shiwei Lan, Wesley O Johnson, and Radford M Neal. Split Hamiltonian Monte Carlo. *Statistics and Computing*, 24(3):339–349, 2014.

Cosma Rohilla Shalizi and Edward McFowlan III. Estimating causal peer influence in homophilous social networks by inferring latent locations. *arXiv preprint arXiv:1607.06565*, 2016.

Susan Shortreed, Mark S Handcock, and Peter Hoff. Positional estimation within a latent space model for networks. *Methodology*, 2(1):24–33, 2006.

Neil A. Spencer. Latentpositionnetworks. <https://github.com/neilspencer/LatentPositionsMCMC>, June 2020.

Neil A. Spencer and Cosma Rohilla Shalizi. Projective, sparse, and learnable latent position network models. *arXiv preprint arXiv:1709.09702*, 2019.

James P Spillane and Megan Hopkins. Organizing for instruction in education systems and school organizations: How the subject matters. *Journal of Curriculum Studies*, 45(6):721–747, 2013.

James P Spillane, Megan Hopkins, and Tracy M Sweet. School district educational infrastructure and change at scale: Teacher peer interactions and their beliefs about mathematics instruction. *American educational research journal*, 55(3):532–571, 2018.

Tracy Sweet and Samrachana Adhikari. A latent space network model for social influence. *Psychometrika*, pages 1–24, 2020.

Tracy M Sweet, Andrew C Thomas, and Brian W Junker. Hierarchical network models for education research: Hierarchical latent space models. *Journal of Educational and Behavioral Statistics*, 38(3):295–318, 2013.

Luke Tierney. Markov chains for exploring posterior distributions. *the Annals of Statistics*, pages 1701–1728, 1994.

John Towns, Timothy Cockerill, Maytal Dahan, Ian Foster, Kelly Gaither, Andrew Grimshaw, Victor Hazlewood, Scott Lathrop, Dave Lifka, Gregory D Peterson, et al. Xsede: Accelerating scientific discovery computing in science & engineering, 16 (5): 62–74, sep 2014. *URL* <https://doi.org/10.1109/mcse>, 2014.

Kathryn Turnbull. *Advancements in latent space network modelling*. PhD thesis, Lancaster University, 2020.

Feng Xie and David Levinson. Modeling the growth of transportation networks: A comprehensive review. *Networks and Spatial Economics*, 9(3):291–307, 2009.

6 Appendix

6.1 Computational Details of Experiments

The implementations of all of the algorithms we used for the empirical studies in Section 4.2 and Section 4.3 have been made public as part of the R package `LatentPositionNetworks` [Spencer, 2020]. The Metropolis within Gibbs algorithms use a multivariate uniform distribution over $[z_i - \delta, z_i + \delta]$ as the proposal distribution q_δ , with δ tuned to target an

acceptance rate within 20 and 30 percent. Similarly, the value of ϵ for the split HMC algorithms was tuned to target an acceptance rate between 80 and 85 percent. The tuned values of ϵ and δ for all of the configurations in Study 1 are available in Figure 6.3.

All experiments (except those involving Stan) were run using the Bridges High Performance Computing System [Nystrom et al., 2015] at the Pittsburgh Supercomputing Center. The computing costs were supported by XSEDE Integrated Advanced Digital Services [Towns et al., 2014]. Because of a software version incompatibility issue, we had to instead run the Stan experiments on a Hydra computing cluster supported by the Department of Statistics and Data Science at Carnegie Mellon University. Timing tests revealed that the Bridges supercomputer runs roughly 3.3 to 3.6 times slower than analogous runs on the Hydra computing cluster. To facilitate direct comparisons between the Hydra and Bridges experiments, all run times of the Stan algorithms were multiplied by a factor of 3.3 when determining the comparisons shown in Figure 1. Version 2.18.2 of `rstan` was used to run the experiment, and `coda` version 0.19-2 was used when calculating effective sample sizes.

6.2 Full Conditional Distributions

Sections 6.2.1 and 6.2.2 provide the details of the targeted joint distribution as well as the relevant conditional distributions and algorithmic steps for split HMC + FlyMC and standard split HMC, respectively.

6.2.1 Split HMC + FlyMC

The full joint distribution of all observed data and parameters for our split HMC + FlyMC strategy (after applying the re-parametrization described in Section 3.3.2) can be decomposed as

$$p(A, U, Z, \theta, \tau, \gamma^2 \mid x, a_*, b_*, \alpha, \beta, \Omega) = p(U \mid \gamma^2, A, \Omega) p(A \mid Z, \theta, \tau, \gamma^2, x) p(Z \mid \gamma^2, \Omega) \quad (46)$$

$$\times p(\theta \mid \tau, x) p(\tau \mid \alpha, \beta) p(\gamma^2 \mid a_*, b_*), \quad (47)$$

where $x \in [C]^{n \times n}$ denotes the observed covariates, $a_*, b_* \in \mathbb{R}_+$ denote the hyperparameters for the inverse gamma prior on γ^2 , $\alpha, \beta \in \mathbb{R}_+^C$ denote the hyperparameters for the beta prior(s) on τ , and Ω denotes the prior covariance for the latent positions Z before the re-parametrization. The full expression for each of the components in the decomposition is

$$p(A | Z, \theta, \tau, \gamma^2, x) = \left(\prod_{\{i,j\} \in E_A} \tau_{x_{ij}} \right) \exp \left(-\frac{1}{2} \sum_{\ell=1}^d Z_{\cdot \ell}^T L_A Z_{\cdot \ell} \right) \prod_{\substack{\theta_{ij}=1 \\ A_{ij}=0}} \left(1 - \exp \left(-\frac{1}{2} \|z_i - z_j\|^2 \right) \right) \quad (48)$$

$$p(Z | \gamma^2, \Omega) = \frac{1}{(2\pi)^{nd/2} \gamma^{nd} \det(\Omega)^d} \exp \left(-\frac{1}{2\gamma^2} \sum_{\ell=1}^d Z_{\cdot \ell}^T \Omega^{-1} Z_{\cdot \ell} \right) \quad (49)$$

$$p(\gamma^2 | a_*, b_*) = \frac{b_*^{a_*}}{\Gamma(a_*)} (\gamma^2)^{-a_*-1} \exp \left(-\frac{b_*}{\gamma^2} \right) \quad (50)$$

$$p(\theta | \tau, x) = \prod_{\{i,j\} \in A} \tau_{x_{ij}}^{\theta_{ij}} (1 - \tau_{x_{ij}})^{1-\theta_{ij}} \quad (51)$$

$$p(\tau | \alpha, \beta) = \prod_{c=1}^C \frac{\Gamma(\alpha_c + \beta_c)}{\Gamma(\alpha_c)\Gamma(\beta_c)} \tau_c^{\alpha_c-1} (1 - \tau_c)^{\beta_c-1} \quad (52)$$

$$p(U | \gamma^2, A, \Omega) = \frac{\det \left(\frac{1}{\gamma^2} \Omega^{-1} + L_A \right)^d}{(2\pi)^{nd/2}} \exp \left(-\frac{1}{2} \sum_{\ell=1}^d U_{\cdot \ell}^T \left(\frac{1}{\gamma^2} \Omega^{-1} + L_A \right)^{-1} U_{\cdot \ell} \right) \quad (53)$$

where $\det(\cdot)$ denotes the determinant of a matrix and $\Gamma(\cdot)$ denotes the Gamma function. To perform MCMC on this distribution, we alternate through the following conditional updates

1. Use split HMC described in Section 3.1 to update (Z, U) according to the conditional posterior density $p(U, Z | A, \theta, \gamma^2, \Omega)$ defined by

$$p(U, Z | A, \theta, \gamma^2, \Omega) \propto \exp \left(-\frac{1}{2} \sum_{\ell=1}^d Z_{\cdot \ell}^T \left(\frac{1}{\gamma^2} \Omega^{-1} + L_A \right) Z_{\cdot \ell} + U_{\cdot \ell}^T \left(\frac{1}{\gamma^2} \Omega^{-1} + L_A \right)^{-1} U_{\cdot \ell} \right) \quad (54)$$

$$\times \prod_{\substack{\theta_{ij}=1 \\ A_{ij}=0}} \left(1 - \exp \left(-\frac{1}{2} \|z_i - z_j\|^2 \right) \right) \quad (55)$$

Note that in this case, the mass matrix for HMC is given by

$$M = \left(\frac{1}{\gamma^2} \Omega^{-1} + L_A \right) \quad (56)$$

which amounts to having it adaptively updated according to γ^2 .

2. Apply the Metropolis-Hastings strategy described in Section 3.2 to update each of θ_{ij} for which $A_{ij} = 0$ according to the conditional posterior density $p(\theta | \tau, x)$ defined by

$$p(\theta_{ij} = 0 | A_{ij} = 0, \tau_{x_{ij}}) = \frac{1 - \tau_{x_{ij}}}{1 - \tau_{x_{ij}} \exp(-\frac{1}{2} \|z_i - z_j\|^2)}. \quad (57)$$

Recall that because $p(\theta_{ij} = 0 | A_{ij} = 1, \tau_{x_{ij}}) = 0$, the θ_{ij} for which $A_{ij} = 1$ need not be updated—they are known to be fixed at one.

3. Apply the Gibbs updates described in Section 3.3.1 to update each entry in τ according to the beta conditional posterior densities

$$p(\tau_c | \theta, \alpha_c, \beta_c) = \frac{\Gamma(\alpha_c + \beta_c + \Theta_c^0 + \Theta_c^1)}{\Gamma(\alpha_c + \Theta_c^0)\Gamma(\beta_c + \Theta_c^1)} \tau_c^{\alpha_c + \Theta_c^1 - 1} (1 - \tau_c)^{\beta_c + \Theta_c^0 - 1} \quad (58)$$

where Θ_0^c and Θ_1^c are defined as in (34) and (35), reproduced below for easy access.

$$\begin{aligned} \Theta_c^0 &= |\{ \{i, j\} \in [n]^2 : \theta_{ij} = 1 \text{ and } x_{ij} = c \}| \\ \Theta_c^1 &= |\{ \{i, j\} \in [n]^2 : \theta_{ij} = 0 \text{ and } x_{ij} = c \}|. \end{aligned}$$

4. Apply the Gibbs update described in Section 3.3.2 to update γ^2 according to the inverse gamma conditional density

$$p(\gamma^2 | a_*, b_*, Z, \Omega) = \frac{\left(b_* + \frac{1}{2} \sum_{\ell=1}^d Z_{\cdot\ell}^T \Omega^{-1} Z_{\cdot\ell} \right)^{a_* + \frac{nd}{2}}}{\Gamma(a_* + \frac{nd}{2}) (\gamma^2)^{a_* + \frac{nd}{2} + 1}} \exp\left(-\frac{\left(b_* + \frac{1}{2} \sum_{\ell=1}^d Z_{\cdot\ell}^T \Omega^{-1} Z_{\cdot\ell} \right)}{\gamma^2}\right). \quad (59)$$

Note that this expression above arises only after marginalizing the momentum variables U . Typically, after such a marginal update in MCMC, the U parameter would need to be updated according to its conditional distribution. In practice, this is not necessary, as U is not one of the target parameters (moreover, the Gibbs update is immediately applied again in the following Step 1).

6.2.2 Split HMC

The full joint distribution of all observed data and parameters for our split HMC strategy (after applying the re-parametrization described in Section 3.3.2) can be decomposed as

$$p(A, U, Z, \tau, \gamma^2 | x, a_*, b_*, \alpha, \beta, \Omega) = p(U | \gamma^2, A, \Omega) p(A | Z, \tau, \gamma^2, x) p(Z | \gamma^2, \Omega) \quad (60)$$

$$\times p(\tau | \alpha, \beta) p(\gamma^2 | a, b), \quad (61)$$

where $x \in [C]^{n \times n}$ denotes the observed covariates, $a_*, b_* \in \mathbb{R}_+$ denote the hyperparameters for the inverse gamma prior on γ^2 , $\alpha, \beta \in \mathbb{R}_+^C$ denote the hyperparameters for the beta prior(s) on τ , and Ω denotes the prior covariance for the latent positions Z before the re-parametrization. The full expression for each of the components in the decomposition is

$$p(A | Z, \tau, \gamma^2, x) = \left(\prod_{\{i,j\} \in E_A} \tau_{x_{ij}} \right) \exp \left(-\frac{1}{2} \sum_{\ell=1}^d Z_{\cdot \ell}^T L_A Z_{\cdot \ell} \right) \prod_{\{i,j\} \notin E_A} \left(1 - \tau_{x_{ij}} \exp \left(-\frac{1}{2} \|z_i - z_j\|^2 \right) \right) \quad (62)$$

$$p(Z | \gamma^2, \Omega) = \frac{1}{(2\pi)^{nd/2} \gamma^{nd} \det(\Omega)^d} \exp \left(-\frac{1}{2\gamma^2} \sum_{\ell=1}^d Z_{\cdot \ell}^T \Omega^{-1} Z_{\cdot \ell} \right) \quad (63)$$

$$p(\gamma^2 | a_*, b_*) = \frac{b_*^{a_*}}{\Gamma(a_*)} (\gamma^2)^{-a_*-1} \exp \left(-\frac{b_*}{\gamma^2} \right) \quad (64)$$

$$p(\tau | \alpha, \beta) = \prod_{c=1}^C \frac{\Gamma(\alpha_c + \beta_c)}{\Gamma(\alpha_c)\Gamma(\beta_c)} \tau_c^{\alpha_c-1} (1 - \tau_c)^{\beta_c-1} \quad (65)$$

$$p(U | \gamma^2, A, \Omega) = \frac{\det \left(\frac{1}{\gamma^2} \Omega^{-1} + L_A \right)^d}{(2\pi)^{nd/2}} \exp \left(-\frac{1}{2} \sum_{\ell=1}^d U_{\cdot \ell}^T \left(\frac{1}{\gamma^2} \Omega^{-1} + L_A \right)^{-1} U_{\cdot \ell} \right) \quad (66)$$

where $\det(\cdot)$ denotes the determinant of a matrix and $\Gamma(\cdot)$ denotes the Gamma function. To perform MCMC on this distribution, we alternate through the following conditional updates

1. Use split HMC described in Section 3.1 to update (Z, U) according to the conditional

posterior density $p(U, Z \mid A, \gamma^2, \Omega)$ defined by

$$p(U, Z \mid A, \gamma^2, \Omega) \propto \exp \left(-\frac{1}{2} \sum_{\ell=1}^d Z_{\cdot \ell}^T \left(\frac{1}{\gamma^2} \Omega^{-1} + L_A \right) Z_{\cdot \ell} + U_{\cdot \ell}^T \left(\frac{1}{\gamma^2} \Omega^{-1} + L_A \right)^{-1} U_{\cdot \ell} \right) \quad (67)$$

$$\times \prod_{\{i,j\} \notin E_A} \left(1 - \tau_{x_{ij}} \exp \left(-\frac{1}{2} \|z_i - z_j\|^2 \right) \right) \quad (68)$$

Note that in this case, the mass matrix for HMC is given by

$$M = \left(\frac{1}{\gamma^2} \Omega^{-1} + L_A \right) \quad (69)$$

which amounts to having it adaptively updated according to γ^2 .

2. Apply a random walk Metropolis to update each entry in τ using its posterior conditional distribution

$$p(\tau_c \mid A, x_{ij}, \alpha_c, \beta_c) \propto \tau_c^{\alpha_c + \zeta_c^1 - 1} (1 - \tau_c)^{\beta_c - 1} \prod_{\substack{x_{ij}=c \\ A_{ij}=0}} \left(1 - \tau_{x_{ij}} \exp \left(-\frac{1}{2} \|z_i - z_j\|^2 \right) \right) \quad (70)$$

where ζ_c^1 is defined as

$$\zeta_c^1 = |\{ \{i, j\} \in [n]^2 : A_{ij} = 1 \text{ and } x_{ij} = c \}|.$$

We recommend updating each entry individually, using a uniform proposal centered at its current value with step-size tuned to obtain an acceptance rate within 20 and 30 percent. This is the strategy we used throughout the article.

3. Apply the Gibbs update described in Section 3.3.2 to update γ^2 according to the inverse gamma conditional density

$$p(\gamma^2 \mid a_*, b_*, Z, \Omega) = \frac{\left(b_* + \frac{1}{2} \sum_{\ell=1}^d Z_{\cdot \ell}^T \Omega^{-1} Z_{\cdot \ell} \right)^{a_* + \frac{nd}{2}}}{\Gamma(a_* + \frac{nd}{2}) (\gamma^2)^{a_* + \frac{nd}{2} + 1}} \exp \left(-\frac{\left(b_* + \frac{1}{2} \sum_{\ell=1}^d Z_{\cdot \ell}^T \Omega^{-1} Z_{\cdot \ell} \right)}{\gamma^2} \right). \quad (71)$$

Note that this expression above arises only after marginalizing the momentum variables U . Typically, after such a marginal update in MCMC, the U parameter would

need to be updated according to its conditional distribution. In practice, this is not necessary, as U is not one of the target parameters (moreover, the Gibbs update is immediately applied again in the following Step 1).

6.3 Additional Figures and Tables

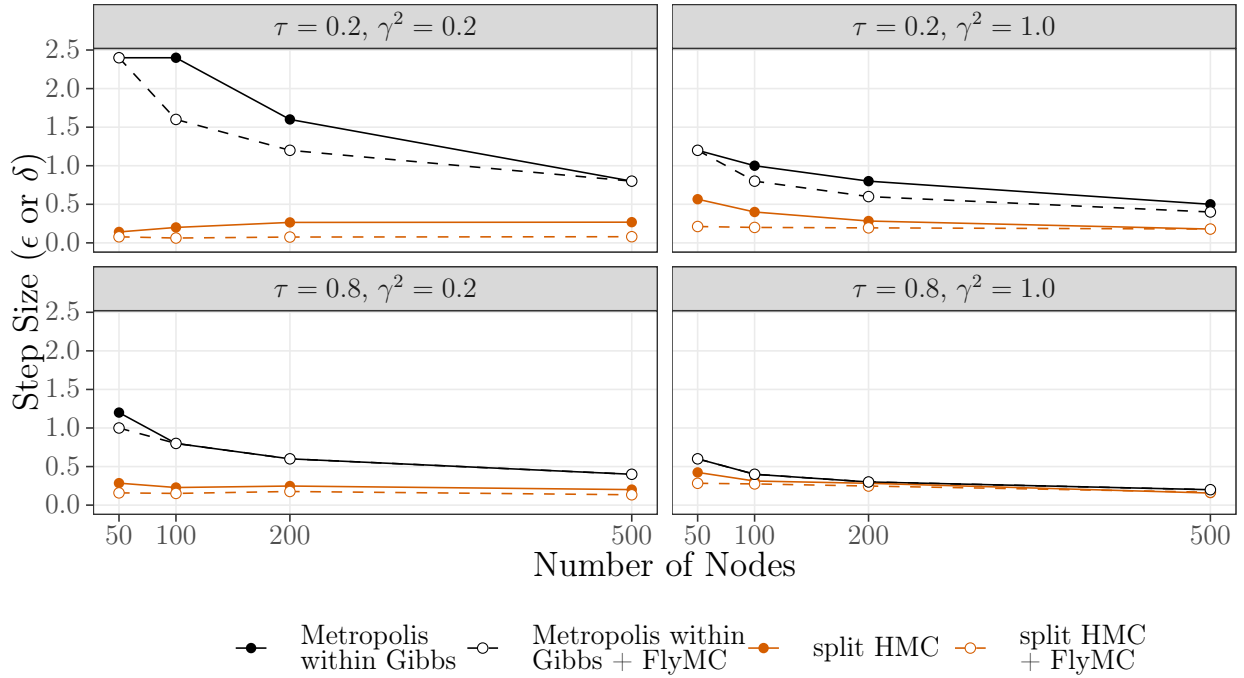


Figure 6: Four panels depicting the tuned step size parameters used for Metropolis within Gibbs, Metropolis within Gibbs + FlyMC, split HMC, and split HMC + FlyMC algorithms used to fit the 16 different networks considered in Study 1 (Section 4.2). Each panel displays the step size parameter (δ for Metropolis methods and ϵ for HMC methods) used for the 50, 100, 200, and 500 node networks generated using the parameter values featured in the panel heading. Point color, point shape, line color, and line shape are used to distinguish between the four algorithms.

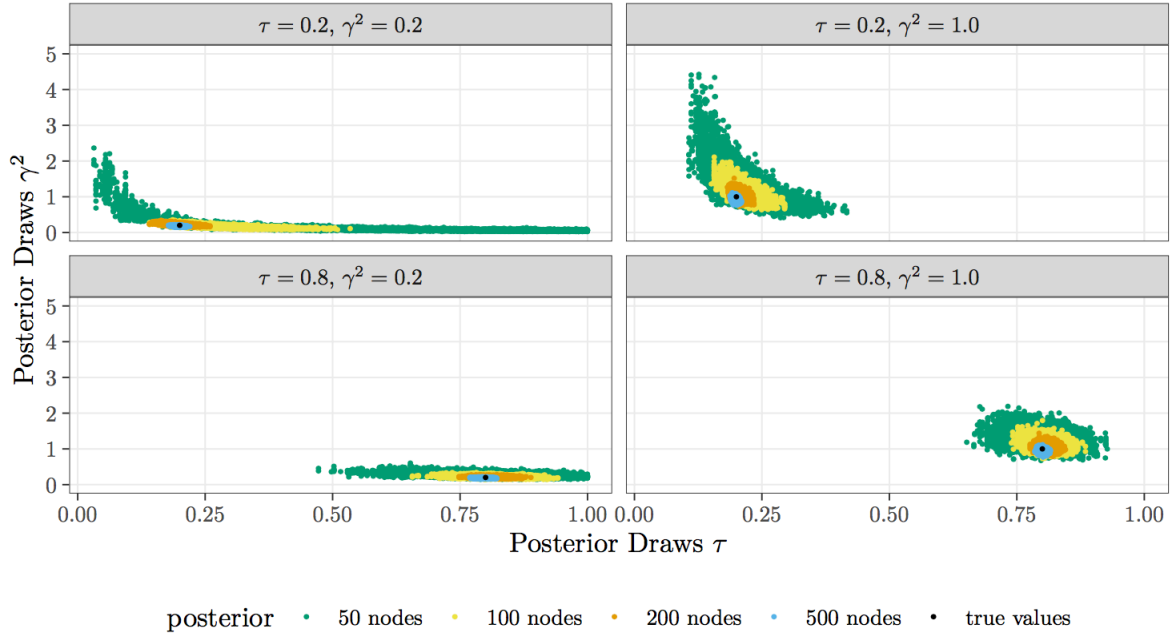


Figure 7: Four panels depicting the marginal joint posterior of τ and γ^2 for the 16 different networks considered in Study 1 (Section 4.2). Each panel displays draws from the joint posterior for the 50, 100, 200, and 500 node networks generated using the parameter values featured in the panel heading. The draws for the networks of different sizes are differentiated by color, with a black point used to indicate the true value of τ and γ^2 used to generate each synthetic network.